Cross-axis Saccade Adaptation in Humans and Marmosets: Behavior and Neurophysiology

by
Simon Orozco

A dissertation submitted to Johns Hopkins University in conformity with the requirements for the degree of Doctor of Philosophy

Baltimore, Maryland
February 2023

© 2023 Simon Orozco
All Rights Reserved

Abstract

The ability to move accurately and maintain that accuracy is one of the most important functions of our brain. We believe that the cerebellum is crucial for this process. This thesis examines the role of the cerebellum in the adaptation of saccadic eye movements during a cross-axis adaptation task. The work began with a careful analysis of eye movements in human subjects and concludes with neurophysiological recordings from the Purkinje-cells (P-cells) of the cerebellar cortex.

In Chapter 2, we examined cross-axis saccade adaptation in human subjects. We found that there seem to be some shared and some independent adaptation processes underlying the early and late parts of saccades. Specifically, learning during the deceleration phase, late in a saccade, is more rapid but also more prone to forgetting than adaptation early in the saccade, during acceleration; however, we found no differences in the retention of learning during error clamp periods or in spontaneous recovery. Further, adaptation following a single error is present only during deceleration. Thus, saccade adaptation may be supported by multiple processes that are expressed at different times during the saccade.

In Chapter 3, we tested cross-axis saccade adaptation in the common marmoset, a small, non-human primate. We found, firstly, that marmosets can indeed successfully perform this task and adapt their saccades. Further, we found clear error responses in the complex spike (CS) rate of the cerebellar P-cells in the oculomotor vermis: P-cells that experienced errors similar to their preferred error direction increased their CS firing rate following an error, whereas P-cells that experienced errors in the opposite direction decreased their CS firing rate. Furthermore, we recorded saccade-related modulation of the P-cell simple spikes (SS), and this modulation changed with adaptation. Specifically, P-cells that experienced errors similar to their preferred error direction decreased their SS modulation as adaptation progressed, but saccade-related SS modulation slightly increased in P-cells that experienced errors in the opposite direction. Thus, there is a clear relationship between the preferred error

directions of the P-cells of the OMV, their CS response to repeated visual errors, and the change in their saccade-related SS activity during saccade adaptation.

Primary Reader and Advisor: Dr. Reza Shadmehr

Secondary Reader: Dr. David Zee

Thesis Committee: Dr. Reza, Shadmehr, Dr. David Zee, and Dr. Yoshiko Kojima

Acknowledgements

Firstly, I wish to thank my PhD advisor Dr. Reza Shadmehr. Immediately after meeting Reza, he encouraged me to pursue science and hired me to work in his lab and began encouraging me to complete a PhD. Reza is an excellent scientist, who is passionate about research and teaching his students to also become great scientists, but more importantly, he is also a great person. As a thesis advisor, he has high standards for your work, but he also cares about each of his students as a person and supports their life and development outside the lab as well. He is, in my opinion, the very best thesis advisor anyone could have. Without his encouragement and support, I never would have begun, let alone finished this graduate degree.

I also wish to thank the other members of my thesis committee, Dr. David Zee and Dr. Yoshiko Kojima. I greatly appreciate them taking time out of their own busy schedules to engage with my thesis project and offer suggestions and insights for its improvement.

Next, I must thank my wife Dr. Angela Orozco for her help and support during this process. On numerous occasions, she stepped up to watch our daughters solo to allow me to work, and she always provids a good sounded board when I need to talk through something. As our family has grown and our life has changed, she and I have always worked to figure it out and thrive together, as I am sure we will continue to do for many more years to come, and I look forward to seeing where the future takes us.

I also want to thank my various labmates over the years Tom Reppert, Scott Albert, Ehsan Sedeghat-Nejad, David Herzfeld, Tehrim Yoon, Kaveh Karbasi, Tara Palin, Jay Pi, Amin Fakharian, Alden Naeem, and Paul Hage. One of the best parts of being part of Reza's lab is the people you work with and the culture of collaboration and friendship Reza has built. I am grateful to all of you for many hours spent discussing our research, troubleshooting experiments, debugging code, piloting tasks for each other, talking about life, and sharing good times in lab and at conferences. You all pushed me to be a better scientist and made the journey much more enjoyable than it would have been without you.

Next, I would like to thank three other scientists whose help and support has been instrumental in my scientific development Dr. Maurice Smith, Dr. James Gordon, and Dr. Robert (Bob) Scheidt. Maurice hired me to work in his lab at Harvard when I was an undergrad and kept me on full-time for a year after graduation; during that time, he was the first one who taught me to go beyond loving and learning science to actually doing science, and for that I will always be immensely grateful. While studying for my master's degree at USC, Dr. Gordon taught me, during his class and via our conversations outside of class, to read the scientific literature more deeply and helped me develop a deep appreciation for and admiration of the classic papers in movement science that serve as the foundations of our own work today. After we met at the Neural Control of Movement conference in Dublin in 2017, Bob became one of my good friends and a mentor from afar during the rest of my PhD. Last summer, when Angela and I decided to move our family to Wisconsin to be closer to family, Bob immediately offered his help and support and sponsored me as a visiting scientist at Marquette University, where he works, and offered me one of the student offices in his lab. His help and support proved vital in finishing my dissertation.

Finally, I would like to thank my siblings and parents. I thank my parents for raising me to be someone who works hard and does things to the best of my ability and for always supporting me throughout my circuitous career path. I thank my siblings for always having my back, being available for vent sessions over the phone and for being the most fun. So many of my best memories are of us all being together.

Table of Contents

Abstract....ii

Acknowledgements....iv

Table of Contents....v

List of Tables....vii

List of Figures....vii

Chapter 1 Introduction....1

1.2 The Two-state Model and Spontaneous Recovery....1

1.3 Cross-Axis Saccade Adaptation....3

1.4 The Role of the Cerebellum and Purkinje Cells....3

Chapter 2 Cross-axis Saccade Adaptation in Humans....4

2.1 Introduction....4

2.2 Results....6

2.2.1 Deceleration period commands adapted with high sensitivity to error but exhibited poor retention....7

2.2.2 Control trials: Deceleration period commands were specific to adapted saccades....11

2.2.3 Both the acceleration and deceleration period commands exhibited spontaneous recovery....13

2.2.4 Alternative models of spontaneous recovery....17

2.2.5 Single trial learning dissociates adaptation in the acceleration and deceleration periods of a saccade....23

2.3 Discussion....26

2.3.1 Potential links to neural mechanisms of adaptation....29

2.4 Methods....31

2.4.1 Ethics Statement....32

2.4.2 General protocol....32

2.4.3 Experiment 1....34

2.4.4 Experiment 2....34

2.4.5 Experiment 3....35

2.4.6 Data analysis....36

2.4.7 State-space models....39

2.4.8 Overview of the state-space model....40
2.4.9 The two-state model....42
2.4.10 Model 1....43
2.4.11 Model 2....44
2.4.12 Behavioral and statistical comparisons of Models 1 and 2....46
Chapter 3 Cross-axis Saccade Adaptation in Marmosets....49
3.1 Introduction....49
3.2 Methods....50
3.2.1. Animals....50
3.2.2 Behavioral protocol....51
3.2.3 Neurophysiology....52
3.2.4 Spike sorting and data processing....52
3.2.5 Data analysis....53
3.3 Results....57
3.3.1 Behavior....57
3.3.2 Neurophysiology....59
3.4 Conclusions....65
Chapter 4 Conclusions and Future Directions....66
Bibliography....69
Curriculum Vitae....76

List of Tables

Table 2.1 Parameter values and confidence intervals for Models 1 and 2.....20

Table 3.1 Recorded units and subpopulations.....60

List of Figures

Figure 2.1 Acceleration and deceleration period commands exhibit some of the properties of the fast and slow system.....6

Figure 2.2 Change in eye velocity during adaptation.....7

Figure 2.3 Acceleration period commands exhibited little or no decay during set-breaks.....10

Figure 2.4 Adapted saccades arrive at an endpoint with a trajectory that is quite different from control saccades that arrive at the same endpoint.....12

Figure 2.5 Both acceleration and deceleration period commands exhibit spontaneous recovery.....14

Figure 2.6 Comparison of adaptation due to horizontal errors and vertical errors in Experiment 2.....15

Figure 2.7 Two models of adaptation.....17

Figure 2.8 Parameter recovery analysis.....19

Figure 2.9 Statistical Model Comparison and Model Recovery Analysis.....22

Figure 2.10 Following experience of a single error, correction of the subsequent saccade was primarily during deceleration.....24

Figure 2.11 Accuracy of error clamp trials.....33

Figure 2.12 Change in horizontal starting position altered saccade displacement, mostly during acceleration.....38

Figure 3.1 Experiment structure.....51

Figure 3.2 Behavioral Results.....57

Figure 3.3 CS-on distributions.....59

Figure 3.4 SS Modulation of the CS-on subpopulation.....60

Figure 3.5 SS Modulation of the CS-off subpopulation.....62

Figure 3.6 SS Modulation of the recombined population.....63

Figure 3.7 CS Response to error.....64

Chapter 1: Introduction

The ability to make accurate movements is essential in virtually every aspect of our daily life. This is particularly true of eye movements [1]. Saccades are the rapid eye movements we make when we change the fixation point of our vision within the visual field. Humans can make up to 3 saccades per second adding up to several thousand per day. However, despite their ubiquity, these rapid eye move ments present a significant challenge for the brain: namely, they are too rapid for visual feedback and correction during the movement so the brain must assess their accuracy and make any corrections after their completion [2,3]. This absence of online feedback makes saccades an excellent model for studying motor control [4]. This dissertation examines the role of the cerebellum in the adaptation of saccades in both humans and non-human primates.

In Chapter 2, we discuss 3 cross-axis saccade experiments in human subjects. We will present evidence from that there may be distinct controllers that contribute to saccade adaptation, one that expresses its adaptation during acceleration and another that expresses its adaptation during deceleration.

In Chapter 3, we explore a similar cross-axis saccade adaptation experiment in the common marmoset, a small non-human primate native to the Amazon Rainforest of Brazil. We will show not only that these animals can successfully adapt their saccades in this task but also that changes in the activity of the purkinje cells in the oculomotor region of the cerebellum supports said adaptation.

Finally, in Chapter 4, we will wrap up and present the conclusions of these sets of experiments.

The two-state model and spontaneous recovery

As stated previously, being able to consistently make accurate movements is vitally important in everyday life. However, the inherent noise of our neuromotor system and changing environmental or physical conditions both present a challenge to the brain in accomplishing that goal. We believe the

brain overcomes this challenge by using a model of the expected movement that should result from any given motor command [5,6]. Building and maintaining such a model requires that the brain continuously monitor both the motor commands and the resulting sensory consequences of those commands, making adjustments to the model when the resulting movement does not match the prediction i.e., there was an error on that movement. We call this process of adjustment motor adaptation.

Several years ago, prior work in the Shadmehr lab posited that motor adaptation can be effectively modeled as the sum of two interacting adaptation processes, one that learns quickly but has poor retention (fast process) and another that learns more slowly but benefits from strong retention (slow process) [7]. This model has proved useful in explaining several motor adaptation phenomena, particularly spontaneous recovery, and inspired other similar models [8–12].

Spontaneous recovery occurs when a previously learned but extinguished pattern of behavior spontaneously returns in the absence of error (or other training stimulus) and has been seen in numerous fields that involve learning and/or conditioning, not only motor control [13–16]. The two-state model was innovative in its ability to explain spontaneous recovery via the different properties of the fast and slow adaptation processes [7]. According to this model, one way spontaneous recovery occurs is that when the previously learned behavior is extinguished, the brain nevertheless retains a memory of it in the slow process but that memory is cancelled out by a competing memory, obtained during the extinction period, in the fast process. Then, when the learning signal is removed, the different decay rates of the two processes give rise to spontaneous recovery: The fast process quickly decays back to zero, while the slow process decays more gradually so that the overall observed behavior reverts toward the previously learned behavior.

Cross-axis saccade adaptation

We have already noted that saccades are an excellent model system for the study of motor control and motor adaptation. Saccades can be adapted via an intra-saccadic target step, i.e. the target is moved to a new location immediately after saccade onset so that when the eye arrives at the original target location the target is no longer there. However, most studies of saccade adaptation traditionally employed either a gain-up (in which the target is jumped further in the same direction as the original saccade) or a gain-down (in which the target is jumped back toward the starting point of the original saccade) perturbation [17–19]. This can make disambiguating the adapted signal from the original motor command difficult. Another way to study saccade adaptation is to jump the target in a direction perpendicular to the original saccade, that is cross-axis saccade adaptation. A previous study from the Shadmehr lab employed this technique and found it to be a powerful tool for studying saccade adaptation [3]. Because the adapted motor commands are perpendicular to the original motor commands, they can easily be isolated and analyzed.

Role of the cerebellum and Purkinje cells

We have noted the importance of accurate movements and the necessity of reliable models in the brain to maintain that accuracy. We believe that such models reside in the cerebellum, Latin for “little brain”, a structure that sits behind and below the rest of the brain [6,20–27]. The cerebellum has connections to every other part of the brain and has been implicated in many neural processes, yet it seems to be of primary importance in the coordination of muscle contractions and the accuracy of goal-directed movements [24,28–31]. However, the exact mechanisms by which the cerebellum achieves movement accuracy are not well understood and remain an open area of research [22,32–36]. This dissertation aims to contribute to this ongoing research and to help elucidate the cerebellar contributions to motor control and adaptation.

Chapter 2: Cross-Axis Saccade Adaptation in Humans

Introduction

As you read this text, your eyes must accurately move from word to word, and from the end of one line to the start of the next. This accuracy is partly due to the cerebellum[37,38], which monitors errors that are made, learns from them, and corrects the motor commands that guide the subsequent saccade[34]. However, this process of adaptation exhibits a remarkable pattern: when the errors induce adaptation, saccade endpoints gradually change, and when the errors reverse direction, inducing extinction, endpoints return to baseline. Yet, following passage of time, and without presence of errors, the saccade endpoints revert back toward the previously adapted state[39,40]. This "spontaneous recovery" is a fundamental feature of many learning paradigms, including classical conditioning[13], fear conditioning[14], and various forms of motor and perceptual learning[7,11,12,15,16,39,41,42]. However, its origin remains a mystery.

A mathematical model[7,43] suggests that during learning, changes in behavior may be supported by two adaptive processes: a fast adaptive process that has high sensitivity to error but suffers from poor retention, and a slow adaptive process that has poor sensitivity to error but benefits from robust retention. In this model, learning followed by extinction produces competition between the fast and the slow processes. Following extinction training, with passage of time the fast process decays, inducing spontaneous recovery of the previously learned behavior. Here, we searched for signatures of these hypothesized processes in saccadic eye movements.

We began with the observation that if the brain experiences a visual error following completion of a saccade (i.e., target is not on the fovea), it learns from that error, producing a change in the motor commands that guide the subsequent saccade[10]. Importantly, the early and the late components of the

eye's trajectory exhibit different patterns of change[3]: whereas the early part of the trajectory adapts little, the late part of the same saccade adapts more. Moreover, with passage of time during set breaks, the early part of the trajectory shows little or no forgetting, but the late part of the same trajectory suffers from more forgetting[3]. Could it be that the slow and fast timescales of adaptation are expressed within different parts of a single movement?

To investigate this question, we induced adaptation by presenting errors that were perpendicular to the primary saccade. This made the adapted commands orthogonal to the original commands, thus allowing for isolation of the learned behavior. As the brain adapted, the response during the acceleration and deceleration phases differed from one another: the acceleration period commands adapted slowly and exhibited robust retention, whereas the deceleration period commands adapted rapidly and exhibited poor retention. Thus, commands during the early and late parts of a single saccade appeared to express certain properties of the hypothesized slow and fast processes.

Next, we performed an experiment in which the perturbations were random. When we isolated the adaptive response to a single error, we made a surprising discovery: following experience of error, the correction to the saccade on the subsequent trial was expressed only during deceleration.

Together, these results suggest that the commands that guide a single saccade may be supported by one adaptive controller that largely contributes to the acceleration period, and another that contributes more to the deceleration period. In principle, spontaneous recovery could arise from the differing error sensitivity and retention properties of these controllers. But when we tested this idea, a third adaptive state emerged, one that appeared to re-aim the saccade's trajectory and was shared across the acceleration and deceleration periods. Spontaneous recovery occurred when this shared state interacted with the slow and fast states expressed during the acceleration and deceleration periods.

Results

We asked healthy human participants (n=101) to make a saccade toward a visual target at 15°. As the primary saccade started, we moved the target perpendicular to the primary movement by 5°, thus presenting a visual error that encouraged adaptation.

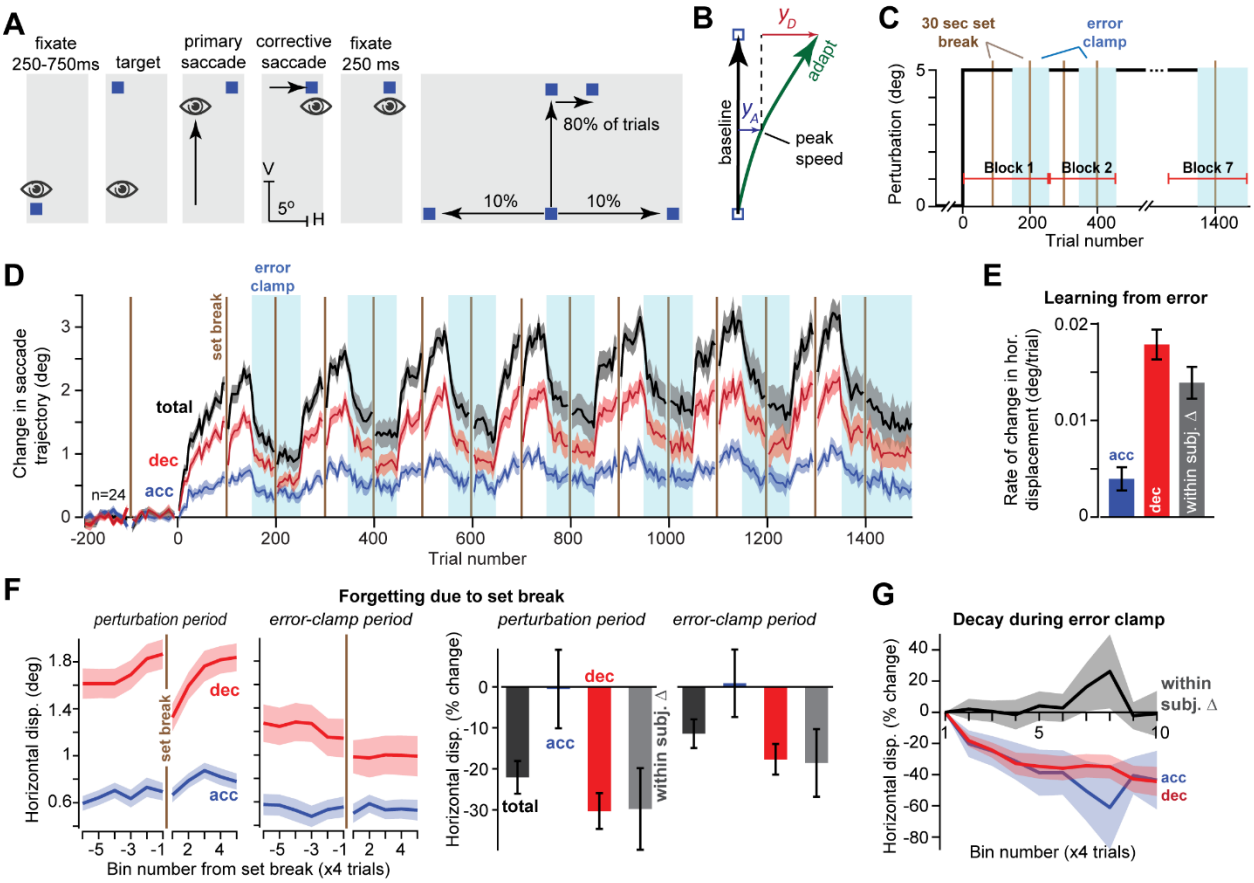


Figure 2.1. Acceleration and deceleration period commands exhibit some of the properties of the fast and slow system. **A**. Experiment 1 trial structure. Following a vertical primary saccade, subjects experienced a rightward horizontal endpoint error. **B**. To quantify adaptation, we measured the horizontal displacement of the adapted saccade with respect to baseline saccades. We integrated horizontal eye velocity over the acceleration and deceleration periods to determine the displacement during each period. **C.** Training blocks. Each block consisted of four periods: initial adaptation, set break (brown line), re-adaptation, error clamp. **D**. Horizontal displacement during the acceleration period was smaller than during the deceleration period, but exhibited little or no forgetting at set breaks. **E**. Trial-to-trial rate of change in the horizontal displacement produced by the acceleration and deceleration period commands during the perturbation blocks. Rate of change was faster in the deceleration period. **F**. Effect of set break on the horizontal displacement in the perturbation blocks and error clamp blocks. At left we show adaptation aligned to set breaks and averaged across all periods. Bin size is 4 trials. Decay was much greater in deceleration period commands. At right, we calculated the percent loss during set breaks in the perturbation and error clamp periods (depicted at left). **G**. Decay in the acceleration and deceleration period commands during the error clamp period. Error bars are between subject SEM. Bin size is 4 trials.

Deceleration period commands adapted with high sensitivity to error but exhibited poor retention

In Exp. 1, participants (n=24) made primary saccades in the vertical direction (80% of the trials, Figure 2.1A). To induce adaptation, after presentation of the target we jumped it horizontally at saccade onset so that the movement ended with an error perpendicular to its primary direction. This error induced adaptation, resulting in a change in the motor commands that guided subsequent primary saccades. We quantified the change in motor commands via the saccade's horizontal velocity (Figure 2.2A), which grew during perturbation trials but decayed during error clamp trials (Figure 2.2D) and following set breaks (30 sec in duration, Figure 2.2B). To analyze these patterns of adaptation, we focused on the time course of each saccade's horizontal velocity.

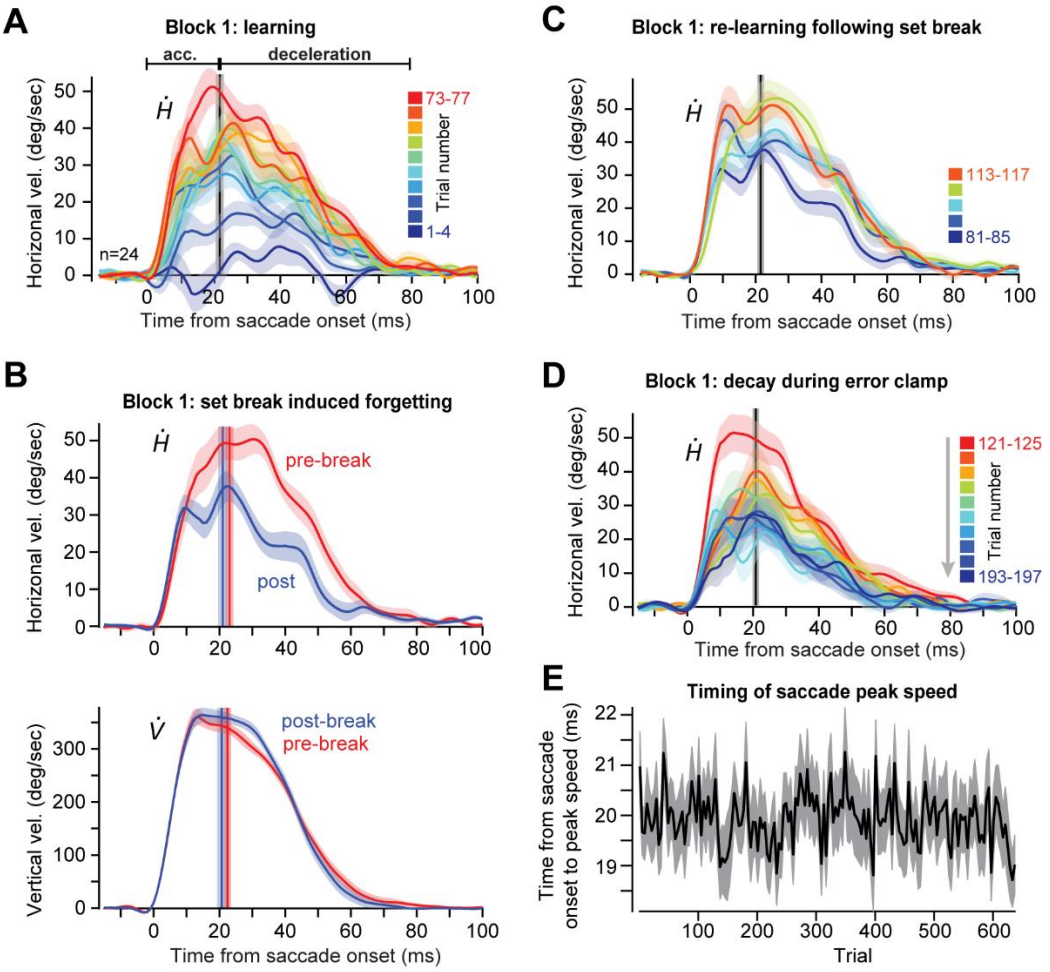


Figure 2.2 Change in eye velocity during adaptation**.** In the main text, we quantified adaptation as the perpendicular displacement of the eye during the acceleration and deceleration phases of the saccade. To calculate this displacement, we integrated horizontal velocity before and after peak speed. Here we show the horizontal velocity during various periods of the first block in Exp. 1. Data are within-subject change in velocity with respect to baseline. Vertical lines indicate timing of peak speed, thus separating the acceleration and deceleration phases of the movement. **A.** Horizontal velocity during the initial adaptation period. **B.** Effect of set break on horizontal and vertical velocities. The set break caused decay in horizontal velocity, primarily during the deceleration period (top). The decay was larger in the deceleration period (-0.11 ± 0.33 deg/sec, t(23) = -0.35, p = 0.73 for the acceleration period, -10.08 ± 2.07 deg/sec, t(23) = -4.88, p = $6.33X10^{-5}$ for the deceleration period). Vertical velocity did not show decay following a set break (bottom, +7.09 ± 2.32 deg/sec, t(23) = 3.06, p = 0.006). **C.** Re-learning after the set break during the first perturbation block. **D.** Decay of horizontal velocity during the first error clamp block. **E**. Timing of peak speed with respect to saccade onset. The timing that categorizes the movement into acceleration and the deceleration phases was computed by the peak speed, which depends on horizonal as well as vertical velocity. Thus, this timing could change over the learning period as the adaptation component increases, influencing the ratio of the two indexes between the acceleration and deceleration phases. We measured the timing of peak speed with respect to saccade onset in Exp. 1 as well as Exp. 2 and found that there were no significant changes in peak speed timing (Exp 1: F(2,69)=0.004, p=0.997; Exp 2: F(3,156)=0.08, p=0.97). Combined data across the two experiments are plotted here. Shaded error regions are between subject SEM.

Our prior work[3] suggested that adaptation produced changes in saccade trajectory that differed between the early and late components of a single movement; the commands that arrived near the end of a saccade adapted nearly twice as much as the commands that initiated the saccade (Figure 2.1B). This suggested that peak speed may be a useful marker to divide a saccade into its early and late periods. Thus, we divided each saccade based on the timing of its peak speed, which remained highly consistent through the entire experiment (Figure 2.2E).

We used the timing of the peak speed to divide each saccade into an acceleration phase and a deceleration phase. Peak speed was defined as $\sqrt{\dot{H}^2 + \dot{V}^2}$, where $\dot{H}$ is horizontal velocity and $\dot{V}$ is vertical velocity. To determine how acceleration and deceleration period commands contributed to the learned response, we integrated the horizontal velocity during each phase of the saccade (Figure 2.1B), yielding the displacement during the acceleration and deceleration periods (Figure 2.1D). The displacement differed across the acceleration and deceleration periods in several ways.

First, deceleration period commands made larger contributions to adaptation than acceleration period commands (Figure 2.1D). Indeed, in response to error, deceleration period commands adapted at

a faster rate (Figure 2.1E) than the acceleration period commands (RMANOVA, trial bin by movement phase interaction, $F(4,92)=13.02$, $p=1.93X10^{-8}$, within subject difference of 0.019 ± 0.003 deg/trial, $t(23)=6.92$, $p=4.72X10^{-7}$).

Second, although deceleration period commands adapted more rapidly, they suffered a substantial loss after a set break (Figure 2.1F, left). To quantify this loss, we calculated the percent change in displacement with respect to before set break onset (Figure 2.1F, right), for each participant that achieved at least 0.25° of adaptation (see Methods) in each movement phase prior to the set break. Indeed, set breaks caused large decay in deceleration period commands. For example, when set breaks occurred during the perturbation trials, we observed 30 ± 4% decay (Figure 2.1F, right, perturbation period, $t(21)=-6.95$, $p=7.24X10^{-7}$). Set breaks during the error clamp trials also produced significant decay (Figure 2.1F, right, error clamp period, -18 ± 4%, $t(19)=-4.73$, $p=0.0001$), but the decay was larger during the perturbation periods (within subject difference of 7 ± 3%, $t(20)=2.38$, $p=0.027$).

In contrast to the deceleration period commands, the acceleration period commands showed a strong resistance to set breaks. During both perturbation periods and error clamp periods, set breaks led to much greater loss in deceleration commands than acceleration commands (Figure 2.1F, right; perturbation period, within subject difference: -29.8 ± 10%, $t(21) = -2.99$, $p = 0.007$; error clamp period, within subject difference: -19 ± 8%, $t(19) = -2.25$, $p = 0.037$). In fact, we detected no significant decay in acceleration period commands in either the perturbation periods (Figure 2.1F, perturbation period, -0.5 ± 9.6%, $t(21)=-0.05$, $p=0.96$) or the error clamp periods (Figure 2.1F, error clamp period, 1 ± 8%, $t(19)=0.11$, $p=0.92$). The stability in the acceleration period commands was also observed when decay was operationalized as the total change in adaptation (in deg) without normalization to the levels before the set break (Figure 2.3B).

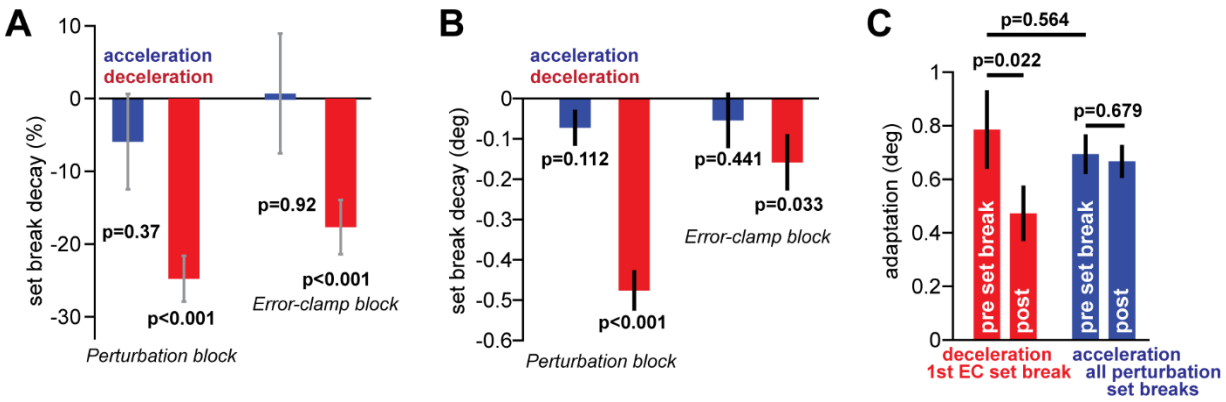


Figure 2.3 Acceleration period commands exhibited little or no decay during set-breaks. Acceleration period commands generally adapted less than the deceleration period commands. This smaller magnitude could have made it more difficult to find significant changes due to set breaks. To check for this, we performed a series of analyses. **A**. Percent change in the perturbation blocks (Exp. 1 and 2), and error clamp blocks (Exp. 1). **B**. Absolute change in the perturbation blocks (Exp. 1 and 2), and error clamp blocks (Exp. 1). **C**. Here we controlled for differences in the adaptation extent exhibited by acceleration and deceleration period commands. We searched for a period in Exp. 1 where deceleration commands were most similar in magnitude to acceleration commands measured throughout the experiment. The optimal period occurred before the first error-camp period, where deceleration commands reached about 0.8 deg (pre-set break deceleration). Acceleration period commands reached about 0.75 deg throughout the experiment (pre-set break acceleration). Regardless, a decay was present in the deceleration period commands but not acceleration.

We were concerned that our inability to detect set break decay in the acceleration period commands may have been because of their small magnitude. Thus, we searched for trials where deceleration period adaptation was as small in magnitude as the acceleration period commands and observed that once again, decay was present in the deceleration period commands but not acceleration (Figure 2.3C).

Surprisingly, while acceleration periods commands exhibited resistance to decay at set breaks, they exhibited substantial decay during the error clamp blocks (Figure 2.1G). Indeed, both the acceleration and deceleration period commands exhibited substantial decay during the error clamp period. In fact, their decay rates did not differ (RMANOVA, main effect of movement phase, $F(1,23) = 0.69$, $p=0.42$, trial by movement phase interaction $F(39,897)=1.27$, $p=0.13$; rates $-0.68 \pm 0.31\%$/trial vs. $-1.17 \pm 0.21\%$/trial; test of within subject difference $t(23)=1.53$, $p=0.14$).

To summarize, the brain learned to alter vertical saccades by generating horizontal commands. However, these horizontal commands were not uniformly expressed during the saccade. Rather, the

deceleration period commands adapted rapidly but exhibited poor retention during set breaks. In contrast, the acceleration period commands adapted slowly but exhibited little or no decay during set breaks. These observations were reminiscent of a two-state model of adaptation, with deceleration commands resembling a “fast state” and acceleration commands resembling a “slow state”. However, there was one aspect of behavior that did not agree with the model: during the error clamp trials, both the acceleration and deceleration period commands decayed at similar rates.

Control trials: deceleration period commands were specific to adapted saccades

At conclusion of training (Fig 1D), in response to a vertical target at (0°,15°) (horizontal and vertical position), the brain generated commands that moved the eyes to (3°,15°); the horizontal commands steered the eyes by roughly 3° as the eyes traveled 15° along the vertical direction. This 3° change in horizontal position of the eyes was largely due to commands that arrived during the deceleration period. With that said, the deceleration period lasted approximately 50 ms, twice as long as the period devoted to acceleration, which lasted approximately 20 ms (Figure 2.2). Could it be that the acceleration period’s smaller contribution to the adaptive response was simply due to its shorter duration?

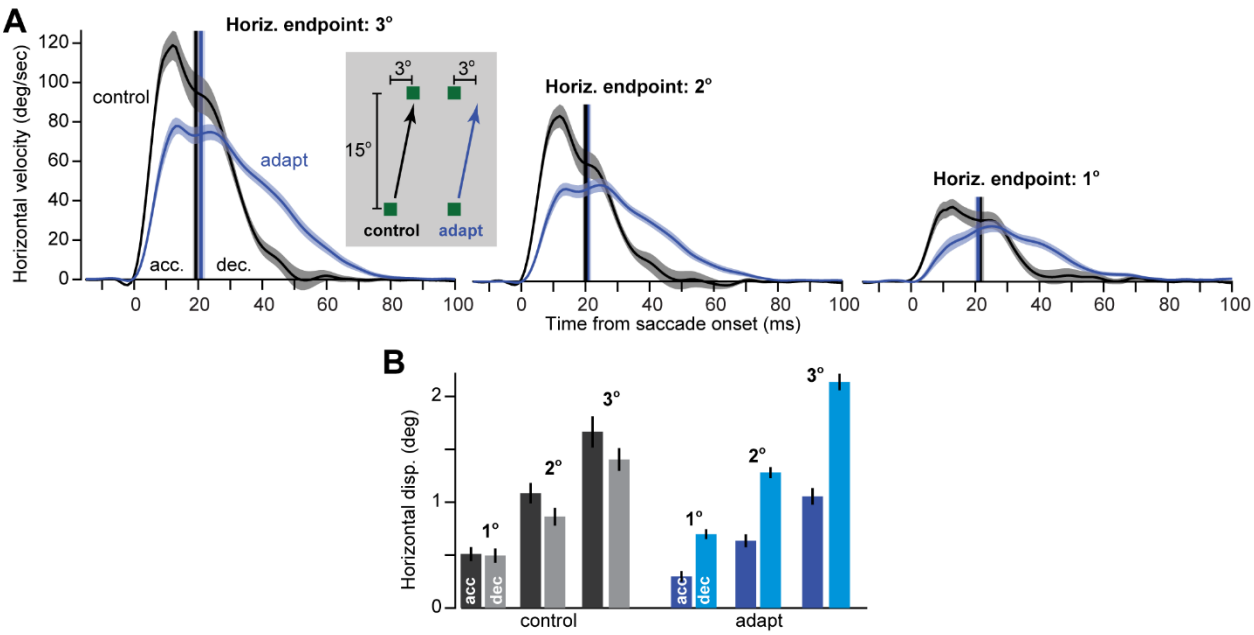


Figure 2.4. In Experiment 1, adapted saccades arrive at an endpoint with a trajectory that is quite different from control saccades that arrive at the same endpoint. **A**. Horizontal velocity of control saccades and adapted saccades. In control trials, targets are presented at (+1°,15°), (+2°,15°), and (+3°,15°). In adapted saccades, the same endpoint is achieved but through learning. Adapted saccades exhibit a smaller horizontal displacement during the acceleration period, but a larger displacement during the deceleration period (with respect to baseline). **B**. Control saccade have roughly equal horizontal displacement for the acceleration and deceleration period commands. In comparison, an adapted saccade has most of its horizontal displacement due to the deceleration period commands. Error bars are between subject SEM.

To consider this possibility, we compared the trajectory of adapted saccades to that of oblique saccades which had the same endpoint and similar acceleration (20.71 ± 1.02ms vs 20.04 ± 0.71ms) and deceleration (54.00 ± 1.56ms vs 49.35 ±1.05ms) periods, but were made in a control condition in which the primary target was presented at (3°,15°) as shown in Figure 2.4A, top-right.

In the control condition (baseline period prior to adaptation), we occasionally presented the target at an oblique location: (1°,15°), (2°,15°), …, or (5°,15°). Figure 2.4A plots the horizontal velocity in the control and adapted conditions, matched across different horizontal displacements. The saccades in the control and adapted conditions differed markedly. The top plot of Figure 2.4A displays horizontal velocities for saccades that ended with a 3° horizontal displacement. In the control condition, the acceleration and deceleration period commands contributed equally to the horizontal displacement. In contrast, in the adapted state, the 3° endpoint displacement was achieved mainly via commands that

arrived in the deceleration period (within-subject 2-way ANOVA, main effect of adaptation vs. control $F(1,23) = 5.80$, $p = 0.02$, main effect of acceleration vs. deceleration $F(1,23) = 1.33$, $p = 0.26$, interaction $F(1,23) = 49.55$, $p = 3.58 \times 10^{-7}$). This pattern repeated across other saccade magnitudes (Figure 2.4B, within subject difference between percent contribution of acceleration and deceleration commands collapsed across 1, 2, and 3 deg endpoints, baseline vs. adapt, $t(23) = 5.13$, $p = 3.42 \times 10^{-5}$).

Therefore, in both control and adapted saccades, the deceleration period lasted roughly twice the length of the acceleration period. However, during control saccades, the endpoint horizontal displacement was due to equal contributions from acceleration and deceleration period commands (Fig 2B, gray bars, deceleration minus acceleration, $-10 \pm 11\%$, $t(23) = -0.91$, $p = 0.37$). In contrast, during adapted saccades, a majority of the endpoint displacement was due to the commands that arrived during the deceleration period (blue bars in Fig 2B, deceleration minus acceleration: $34 \pm 5\%$, $t(23) = 7.12$, $p = 2.98 \times 10^{-7}$). Thus, even though the oculomotor system could have accomplished the desired horizontal displacement using equal contributions from acceleration and deceleration, as it did in the control condition, during adaptation it was somehow limited to expressing its contributions mainly during deceleration.

Both the acceleration and deceleration period commands exhibited spontaneous recovery

Experiment 1 suggested that acceleration and deceleration commands resembled the slow and fast states of adaptation. In the framework of the two-state model, during extinction the fast state must compete with the slow state, thus resulting in spontaneous recovery [8]. We tested this possibility in Experiment 2.

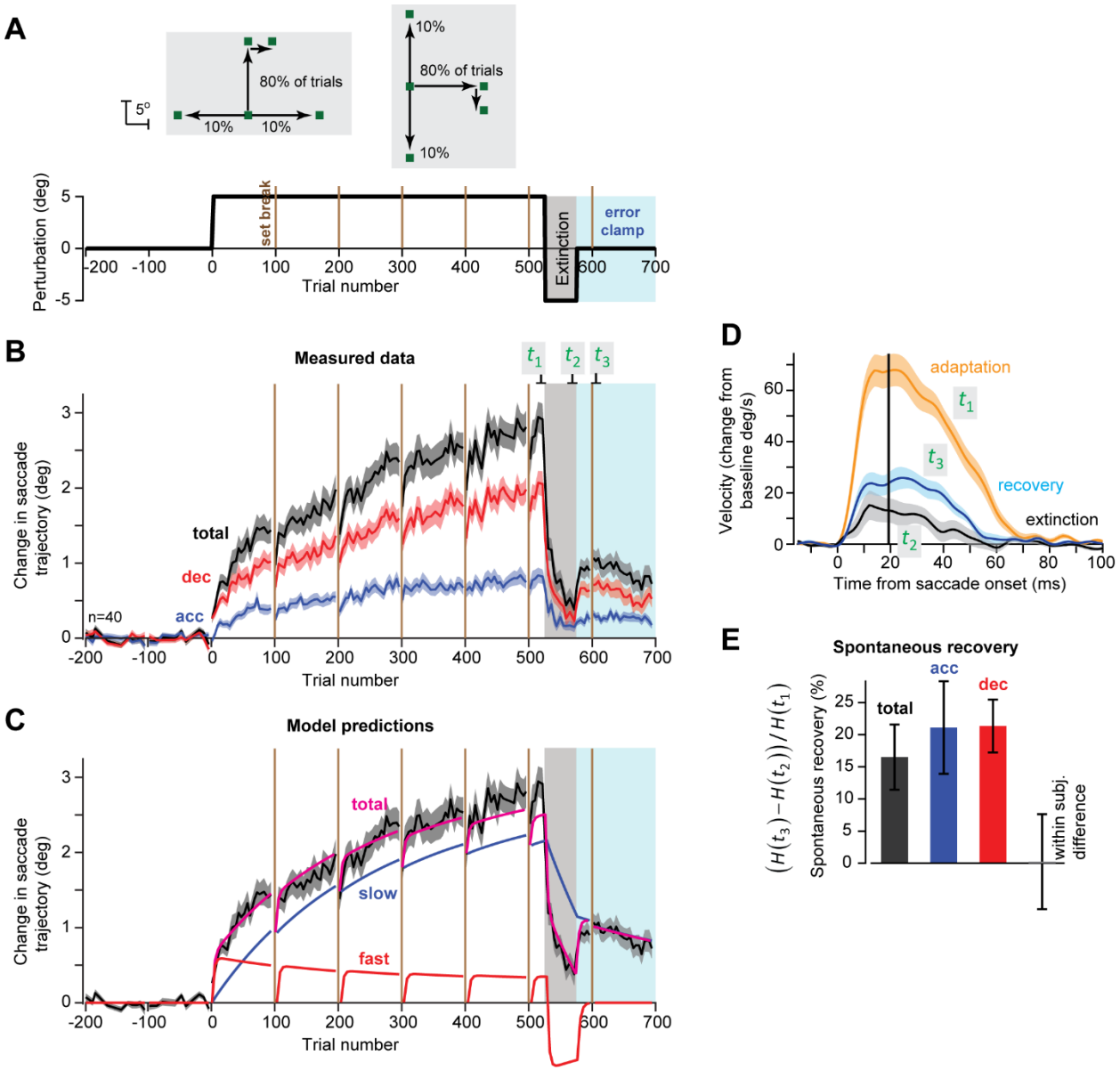


Figure 2.5 Experiment 2. Both acceleration and deceleration period commands exhibit spontaneous recovery. **A**. Experimental design. Perturbation block was followed by an extinction block, and then a block of error clamp trials. Half of the subjects experienced horizontal errors following vertical saccades (left panel), while the other half experienced vertical errors following horizontal saccades (right panel). **B**. Measured data. **C**. A standard two-state model was fit to the measured data (trace labeled total). The fast and slow states that are predicted by the model are shown. **D**. Eye velocity in the direction of error during the trials at end of adaptation (t_1), at end of extinction (t_2), and during error clamp (t_3). **E.** Spontaneous recovery, defined as $[H(t_3) - H(t_2)]/H(t_1)$.

Subjects (n=40) made primary saccades to a target at 15°, and then experienced a +5° error perpendicular to the direction of the target (Figure 2.5A). We then reversed the perturbation direction (-5°) to encourage extinction of the acquired memory. After this extinction phase, a block of error clamp trials followed to assess spontaneous recovery. In separate groups of subjects, we tested adaptation to

horizontal and vertical errors (Figure 2.6A). While horizontal errors induced greater learning, behavior was qualitatively similar across groups (Figure 2.6), and thus the two groups were combined in Fig 2.5.

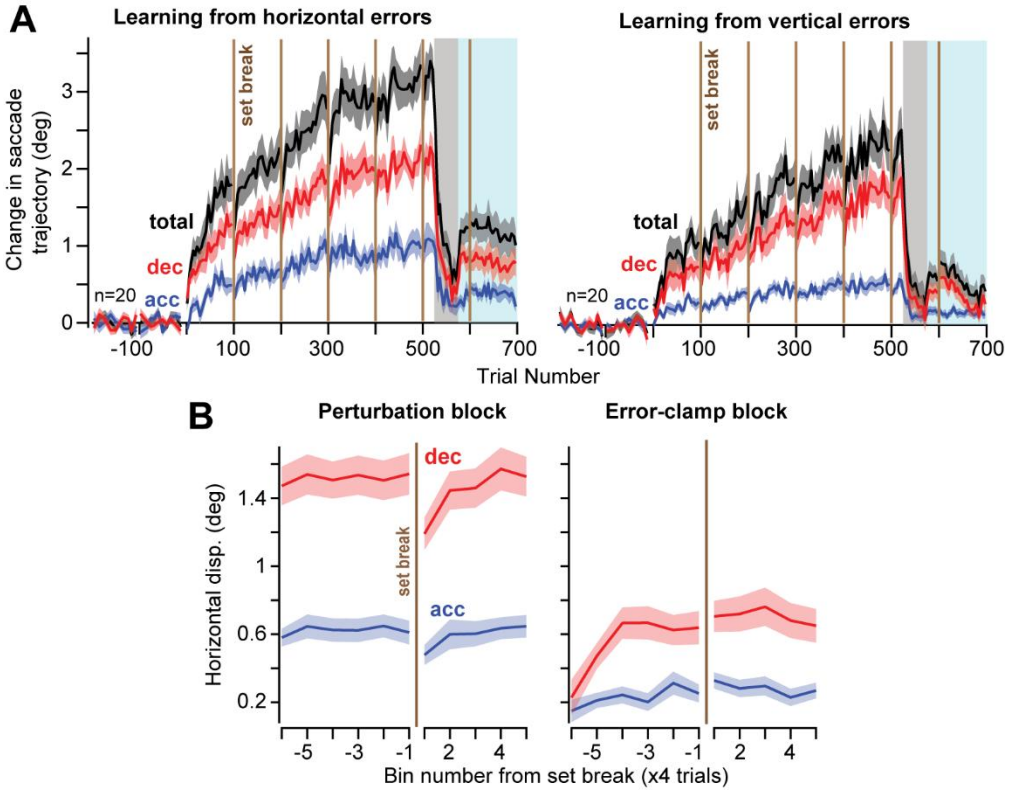


Figure 2.6 Comparison of adaptation due to horizontal errors and vertical errors in Experiment 2. In Experiment 2, an initial perturbation block was followed by extinction and concluded with a block of error clamp trials. Half of the subjects experienced horizontal errors following vertical saccades (left panel), while the other half experienced vertical errors following horizontal saccades (right panel). **A**. Learning in response to horizontal (left panel) and vertical (right panel) errors. Subjects learned somewhat more from horizontal errors than from vertical, especially during the acceleration period (overall rate of change, 0.005 ± 0.0004 deg/trial vs. 0.002 ± 0.0002 deg/trial, within subject difference t(39) = 7.32, p = $7.89X10^{-9}$). **B**. Effect of set breaks during perturbation and error clamp periods, collapsed across all horizontal error subjects and vertical error subjects. Deceleration period commands decayed more than acceleration period commands during the perturbation period (within subject difference: -0.22 ± 0.07°, t(39) = -3.34, p = 0.001), but neither exhibited decay during the error clamp period, as expected during spontaneous recovery.

At the end of the initial +5° perturbation period, saccade endpoint had changed by roughly 3° (trials labeled t_1, Figure 2.5B, black). Reversing the direction of the visual error encouraged extinction, and by the end of the extinction trials endpoint displacement was less than 0.5° (trials labeled t_2, Figure 2.5B). In the error clamp period that followed, the saccades exhibited spontaneous recovery: endpoint displacement with respect to the target increased from 0.5° to around 1° (from t_2 to t_3, Figures 2.5B &

2.5D). We quantified spontaneous recovery as the change in displacement from end of extinction trials (time t_2) to the error clamp block (time t_3) scaled by the level of adaptation at t_1: $[H(t_3) - H(t_2)] / H(t_1)$. Saccade endpoint exhibited roughly 16.5% spontaneous recovery ("total", Figure 2.5E, t(34)=3.26, p=0.002).

We next considered how well the standard two-state model could account for the measured data. We fit the model to the total displacement that we had measured on each trial (Fig 2.5C, magenta) and asked whether the fast and slow states of the model could match the acceleration and deceleration period commands. The observed data differed markedly from the model's states. Whereas the model predicted that performance in the late stages of training would be dominated by the slow state, the observed behavior was in fact dominated by the deceleration period, a putative fast state. More importantly, while the model predicted that spontaneous recovery was due to differential decay in the slow and fast states, the data showed something entirely different: both acceleration and deceleration periods exhibited spontaneous recovery (Figures 2.5D & 2.5E; 21±7%, t(34) = 2.93, p=0.006 and 21±4%, t(34) = 5.19, $p=9.87X10^{-6}$ respectively). Indeed, spontaneous recovery did not differ for the acceleration and deceleration periods (Figure 2.5E; within subject difference, 0.24±7%, t(34) = 0.03, p = 0.97).

In summary, when extinction training followed adaptation, in the subsequent error clamp trials there was spontaneous recovery of saccade endpoints toward the initially learned behavior. However, this was not caused by differential decay patterns in the acceleration and deceleration commands. Rather, the commands during both periods exhibited spontaneous recovery. Thus, despite the fact that acceleration period commands adapted slowly and exhibited resistance to decay, and deceleration period commands adapted rapidly but were susceptible to decay, their dynamics during extinction and spontaneous recovery were inconsistent with the standard 2-state model.

Alternative models of spontaneous recovery

To better understand the results, we considered two possibilities. In Model 1 (Figure 2.7A), we imagined a single adaptive controller with multiple timescales of learning. In this scenario, a fraction of the learning was expressed during acceleration, while the remainder was expressed during deceleration. This model is akin to the one suggested in Chen-Harris et al.[3]: a forward model monitors the ongoing motor commands and corrects the movement as it takes place. Adaptation results in changes in both the acceleration and deceleration phases, but because the deceleration phase is longer, a greater fraction is expressed later.

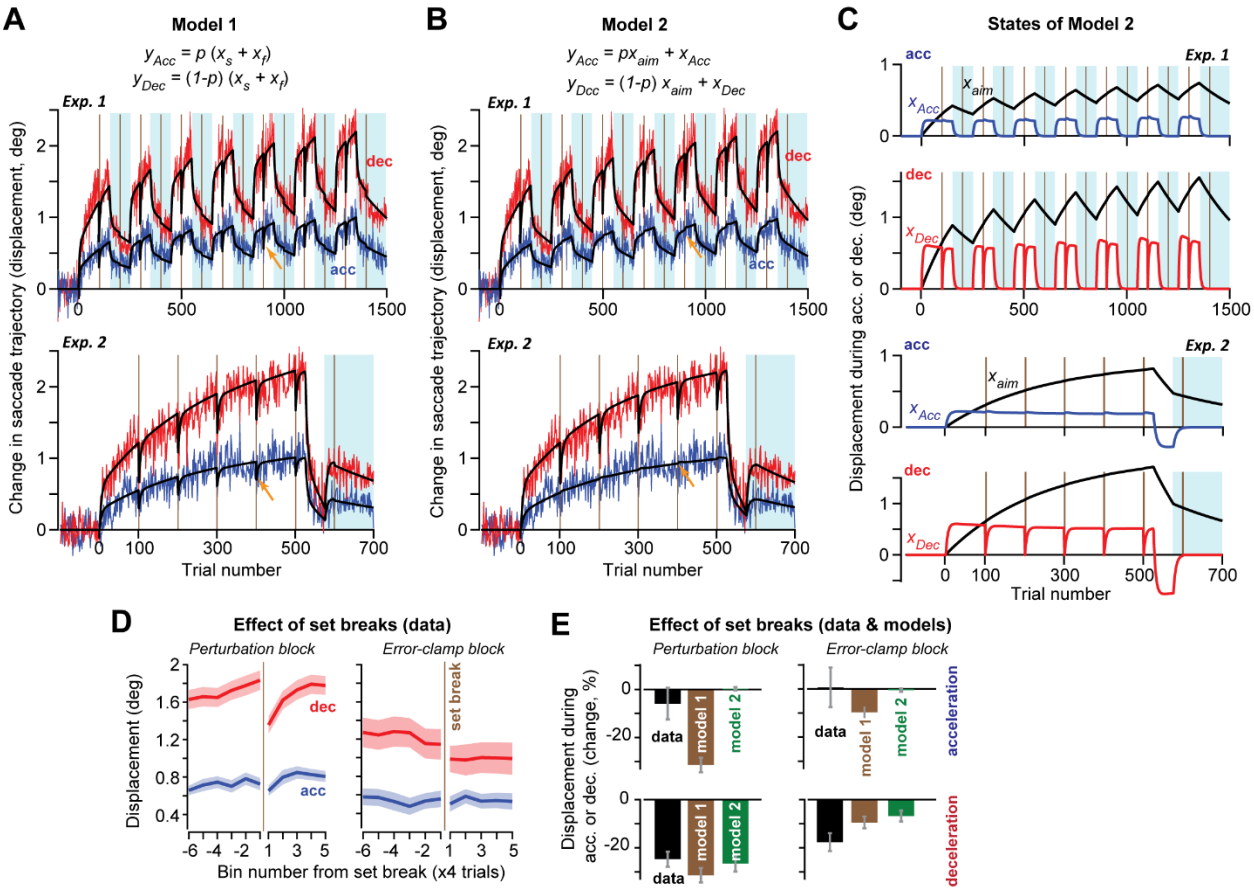


Figure 2.7. Two models of adaptation. **A**. Model 1 represented a single controller that learned from error via a fast state x_f and a slow state x_s. During a saccade, a fraction of the sum of the two states was expressed during acceleration, and the remainder was expressed during deceleration. Arrow indicates the effect of set break on the model's acceleration period commands. **B**. Model 2 relied on two controllers, one that aimed the saccade with state x_{aim}, and another that independently affected the commands during the acceleration and deceleration periods. **C**. States of Model 2 during Exps. 1 and 2. Model 2 could account for the observation that set breaks

produced a loss in the deceleration period but not the acceleration period commands. In addition, Model 2 accounted for the observation that decay following a set break differed in perturbation vs. error clamp trials: note the difference in x_{Dec} at set breaks during perturbation and error clamp blocks of Exp. 1). **D**. Measured set break decay data. Adaptation is shown aligned to set breaks during perturbation periods in Exps. 1 and 2 (left) and error clamp periods in Exp. 1 (right). **E**. Comparison of the set break effects in the models and the measured data. The models differed in their ability to account for acceleration period set break decay. Error bars for data are SEM. Participants from Exps. 1 and 2 were combined when analyzing the perturbation block set breaks. For error clamp block set breaks, only participants from Experiment 1 were used.

A critical component of Model 1 was that learning and forgetting were coupled in the two parts of the movement. For example, if there was partial forgetting that affected the deceleration period, it would also affect the motor commands during the acceleration period. Because this aspect of the model was inconsistent with our data, we considered a variant. In Model 2 (Figure 2.7B), we imagined two controllers that each had a single timescale of learning. One controller learned to aim the saccade toward a new location, and another learned to independently modulate commands during the acceleration and deceleration periods.

We used state-space equations to represent Models 1 and 2 (see Methods). These models were parametrized with error sensitivities, retention factors, and set break decay factors for each state (two states in Model 1, three states in Model 2). Furthermore, because error sensitivity increased with long exposures to consistent errors[44], we allowed error sensitivity to increase over time in both Models 1 and 2. Overall, Models 1 and 2 had 9 and 13 parameters, respectively. Given the high dimensionality of Model 2, we used BIC to reduce its complexity, arriving at 9 parameters (i.e., the rate at which error sensitivity increased was equal across all states, and no parameters were provided to allow for set-break decay in aim or acceleration states). As a result, Models 1 and 2 had the same number of parameters: 9. Ultimately, our ability to recover model parameters was high, according to a parameter recovery analysis (Figure 2.8).

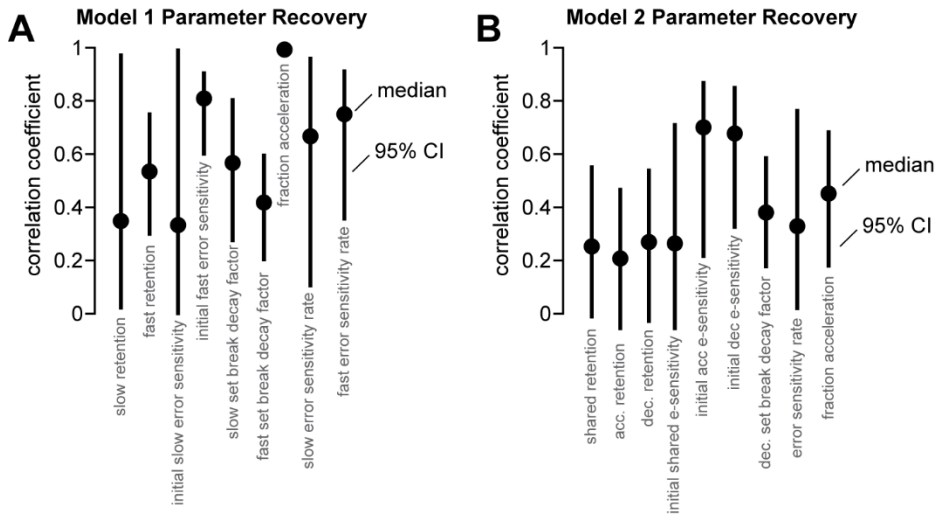


Figure 2.8 Parameter recovery analysis. Models 1 and 2 were fit to individual participants in Exp. 1 and Exp. 2, and then used in a parameter recovery analysis. This analysis was conducted via a bootstrapping approach with 1000 batches. In each batch, each parameter set (n=64 total) was used to simulate noisy behavior with Model 1 (**A**) or Model 2 (**B**). Then Models 1 and 2 were fit to the simulated noisy data for each participant. The parameters recovered by each model were compared with the true underlying parameters. To compare the true parameters with the recovered parameters, we calculated Pearson's correlation coefficient across the 64 participants simulated in a given batch. We repeated this process 1000 times, varying the seed for the random number generator used in each noisy simulation. We then computed the median correlation coefficient, as well as 95% confidence intervals, for each parameter in Models 1 and 2. The higher this correlation, the better the fitting robustness. Black dots represent the median correlation coefficient across 1000 simulated batches, and lines represent 95% confidence intervals.

In Model 1 (Figure 2.7A), there was a single controller that learned from error via a fast state and a slow state. During a saccade, a fraction of the sum of these two states was expressed during acceleration, and the remainder was expressed during deceleration. Thus, this model suggested that faster adaptation during the deceleration period was simply because the deceleration period was longer in duration than the acceleration period. We fit the model to the data in both Experiments 1 and 2. Model 1 was able to reproduce many features of the data. For example, the deceleration period commands adapted more rapidly than the acceleration period commands. This was because in the model, only 31% of learning (sum of fast and slow states) was expressed during acceleration (p = 0.31, Table 1), a value that is similar to the proportion of movement duration due to acceleration (0.28). As expected, the fast state had greater sensitivity to error (as compared to the slow state), but also

suffered from greater trial-to-trial forgetting. Thus, Model 1 could account for the fact that both acceleration and deceleration period commands exhibited spontaneous recovery.

Model 1		
Parameter name	**Mean value**	**95% CI**
a_{slow}	0.9963	[0.9947,0.9996]
a_{fast}	0.8071	[0.7366,0.9387]
$b_{slow,0}$	0.002852	[0.001999,0.003714]
$b_{fast,0}$	0.03267	[0.01228,0.04905]
d_{slow}	0.9481	[0.8721,1]
d_{fast}	0.0599	[6.9×10^{-6},0.573]
p	0.3127	[0.279,0.3469]
β_{slow}	7.844×10^{-6}	[9.154×10^{-15},1.4×10^{-5}]
β_{fast}	9.397×10^{-5}	[3.462×10^{-5},0.000186]
Model 2		
a_{aim}	0.9817	[0.828489,0.998409]
a_{acc}	0.8680	[0.724270,0.995977]
a_{dec}	0.8433	[0.748168,0.999965]
$b_{aim,0}$	0.0051	[0.001831,0.029825]

$b_{acc,0}$	0.0063	[0.001065,0.013130]
$b_{dec,0}$	0.0199	[0.001520,0.031114]
d_{dec}	0.1680	[0,0.861970]
β	0.0027	[0.001004,0.004862]
p	0.3088	[0.190674,0.363140]

Table 1. Parameter values and confidence intervals for Models 1 and 2.

However, set breaks revealed a critical limitation of Model 1. Because acceleration and deceleration were derived from the same adaptive states, when adaptation decayed during deceleration, so too did adaptation during acceleration. However, in the measured data the set breaks during perturbation periods led to decay in only the deceleration period commands (Figure 2.7E, Exps. 1&2 deceleration commands -25 ± 3%, $t(39) = -7.85$, $p = 1.50X10^{-9}$; acceleration commands -6 ± 7%, $t(39) = -0.90$, $p = 0.37$). Similar patterns were observed in response to error clamp period set breaks (Figure 2.7E, data, Exp. 1; deceleration: -18 ± 4%, $t(19)=-4.73$, $p=0.0001$; acceleration: 1 ± 8%, $t(19)=0.11$, $p=0.92$). In summary, while Model 1 generally fit the data well, it could not account for the differential patterns of decay that were present following set breaks.

As expected, Model 2 was able to account for spontaneous recovery, but critically, it was also able to reproduce behavior during set breaks. When set breaks occurred, acceleration period commands of Model 2 showed little decay, whereas deceleration period commands showed substantial decay (Figure 2.7E). The model also agreed with the data in that set breaks produced greater decay during perturbation periods than during error clamp periods (within-subject difference of 7 ± 3%, $t(20)=2.38$, $p=0.027$).

To understand these patterns, we examined the adaptive states predicted by Model 2 (Figure 2.7C). When the set breaks occurred during the perturbation block, the deceleration state was non-zero and therefore exhibited decay. However, when the set breaks occurred during the error clamp block, the same state had substantially decayed prior to the set break, thus limiting additional decay that could occur due to the set break. As a result, set breaks produced different levels of decay during perturbation and error clamp blocks.

Statistical model comparison (log-likelihood) suggested that 47 participants (73.4%) were better described by Model 2, whereas 17 participants (26.6%) were better described by Model 1 (Figure 2.9A). These patterns were recapitulated by a model recovery analysis (Figure 2.9B); when data were simulated with Model 1, log-likelihoods recovered Model 1 with about 55% probability, exceeding the rate observed in the actual data (26.6%) by about 30%. However, when data were simulated with Model 2, log-likelihoods recovered Model 2 with about 80% probability, in close agreement with the rate observed in the actual data (73.4%).

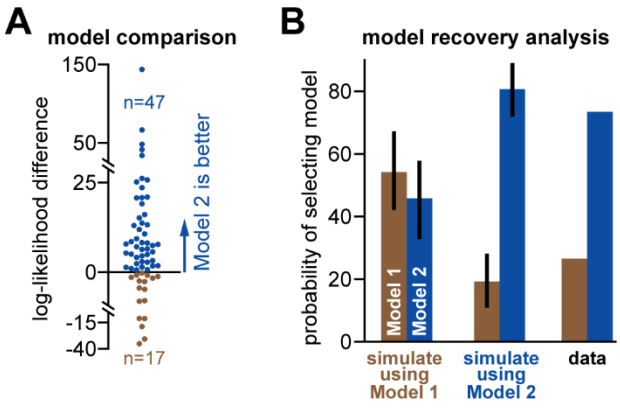


Figure 2.9 Statistical Model Comparison and Model Recovery Analysis. **A.** We calculated the log-likelihood for observing each participant's data given Model 1 and Model 2. In panel **A** we subtract these two likelihoods for each participant: positive values indicate that Model 2 is more likely to explain the participant's data. **B.** We performed a model recovery analysis to determine if the log-likelihood was biased toward either Model 1 or 2, given the design of Experiments 1 and 2. We used a simulation to produce data either with Model 1 or 2, and then calculated the log-likelihood for the true model and the opposing model. For each simulation, we calculated the fraction of participants that BIC or AIC selected for a given model. We did this process 1000 times, each time re-simulating behavior for each subject. At left we simulated the experiments using Model 1. In the middle we simulated the experiments using Model 2. At right we show the probability that a participant was better described by Model 1 or Model 2 in the actual data. This model recovery analysis demonstrated that AIC and BIC were both dependable measures that could be used for model comparison; when data were simulated with Model 1, the log-likelihood measure was more likely to recover Model 1. When data were simulated with Model 2, the log-likelihood measure was more likely to recover Model 2. The bars show the mean. Lines indicated 95% confidence intervals across the 1000 simulations batches.

In summary, we compared two models that could potentially account for patterns of learning and spontaneous recovery. In Model 1 we assumed that there was a single adaptive controller with fast and slow states, but only a portion of its learning was expressed during acceleration, with the remainder during deceleration. In Model 2 we imagined two controllers that each had a single timescale of learning, with one controller learning to aim the saccade toward a new location, and another learning to independently modulate commands during the acceleration and deceleration periods. While both models could account for the data quite well, one critical feature of the data was more consistent with Model 2: the fact that set breaks produced forgetting in the deceleration commands, but not acceleration commands.

Note however that these findings should be interpreted cautiously, as they rely on a null result: the inability to detect set break decay in acceleration period commands. With that said, this result was robust across several analysis methods: (1) in normalized set break decay measures (Figure 2.1), (2) in non-normalized set break decay measures (Figure 2.3B), and when controlling for acceleration and deceleration magnitudes (Figure 2.3C). Thus, overall, the data suggested that acceleration period commands exhibited a resistance to decay that was only captured by Model 2.

Single trial learning dissociates adaptation in the acceleration and deceleration periods of a saccade

A critical element of our analysis was to divide a saccade's trajectory based on its peak velocity, producing measures of adaptation during periods of acceleration and deceleration. However, is this division warranted? That is, is there anything special about the adaptation capabilities of the commands that arrive specifically during deceleration? To answer this question, we performed a new experiment in which we aimed to emphasize adaptation in the fast states of learning, testing whether the result would dissociate the commands between acceleration and deceleration.

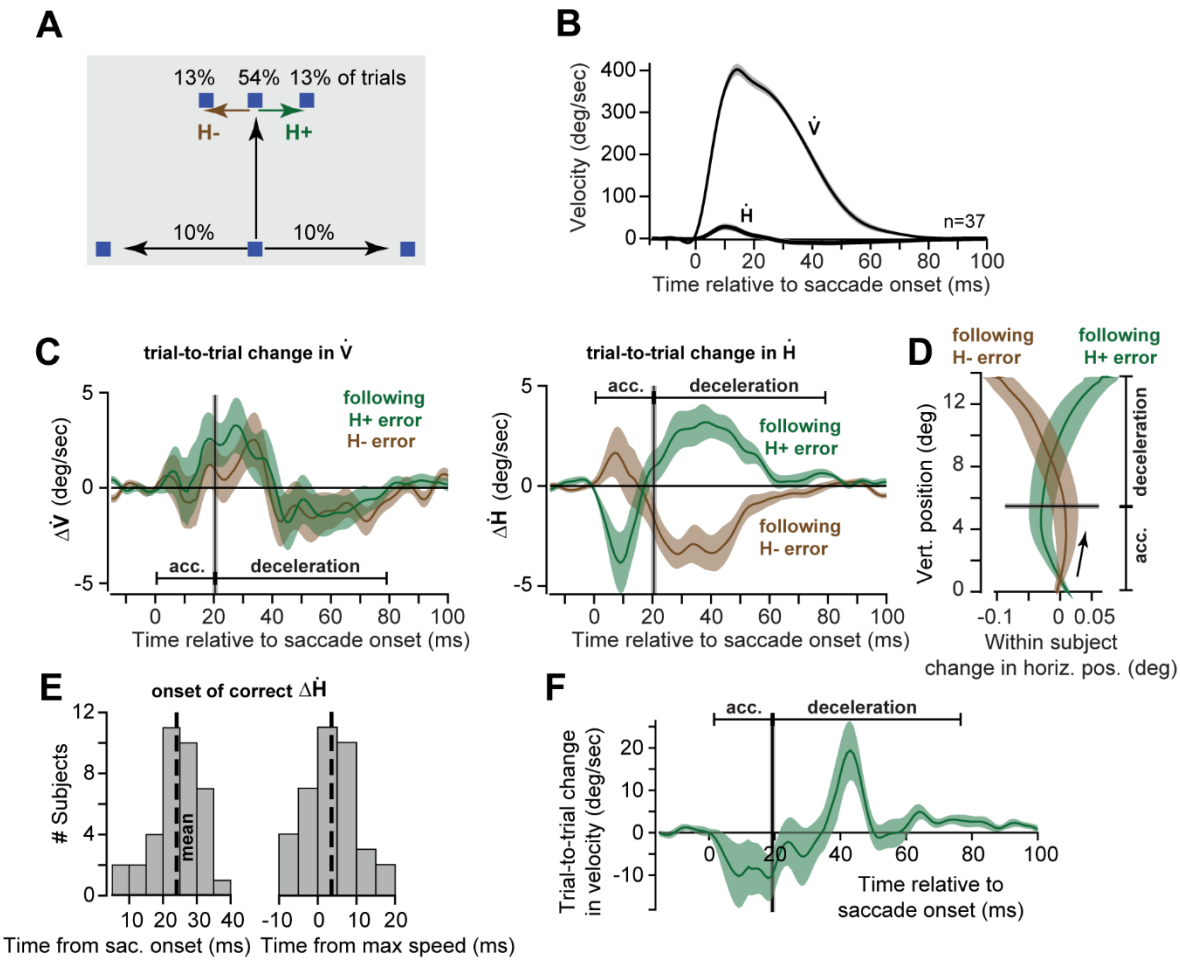


Figure 2.10. Experiment 3. Following experience of a single error, correction of the subsequent saccade was primarily during deceleration. **A**. Subjects made vertical saccades and occasionally experienced a horizontal error. **B**. Average horizontal and vertical velocity of the saccade for the target along the vertical axis. **C**. Trial-to-trial change in vertical and horizontal velocity following experience of a positive or negative horizontal endpoint error. Vertical line indicates time of peak speed, thus separating the acceleration and deceleration periods. **D**. Trial-to-trial change in saccade trajectory following experience of a positive or negative horizontal endpoint error. The endpoint correction was primarily due to commands in the deceleration period. Note the large difference in the scales of the x and y axes. **E**. Onset time of correction in the horizontal velocity following experience of a horizontal endpoint error. Mean onset time is about 3 ms following start of the deceleration period. **F**. Data from Experiments 1 and 2, measuring the response following the experience of error on the very first trial (velocity on trial 2 minus trial 1, in the direction of the perturbation). Shaded error regions are between subject SEM.

In Exp. 3, participants (n=37) made primary saccades in the vertical direction (80% of the trials; Figure 2.10A): during the primary saccade, the target was displaced horizontally to the right or left at random and with equal probability (13% of trials in each case, Figure 2.10A). To measure learning from error, we considered pairs of trials, *n* and *n*+1, in which the primary saccade was to the vertical target, but the target was jumped only in trial *n*. Learning from error was measured as the trial-to-trial change

in the horizontal and vertical eye velocity ($\Delta\dot{H}$ and $\Delta\dot{V}$) of the primary saccade, that is: $\Delta\dot{H}(t) = \dot{H}^{(n+1)} - \dot{H}^{(n)}$.

As expected, there was no error-dependent change in vertical velocity (left panel of Figure 2.10C): in the deceleration period, there was a slight increase in vertical velocity, but the effect did not differ between H^+ and H^- errors (peaks of 5.94 ± 0.77 vs. 5.27 ± 0.57 deg/sec, respectively, t(36) = -0.82, p=0.42). In sharp contrast, the change in horizontal velocity following experience of a horizontal endpoint error was bimodal and differed between acceleration and deceleration. For example, following a positive error H^+, $\Delta\dot{H}$ was negative during the acceleration phase of the primary saccade, thus pulling the eyes in the wrong direction with respect to the error (green trace, right panel of Figure 2.10C). However, during the deceleration period, $\Delta\dot{H}$ became positive, pulling the eyes in the direction that compensated for the error. A similar bimodal pattern was present following experience of H^- error (brown curve, right panel of Figure 2.10C).

The effect of this one-trial learning on eye trajectory is displayed in Figure 2.10D. Experience of an error to the right (H^+, green trace, Figure 2.10D) was followed by a primary saccade that during acceleration changed the eye trajectory in the wrong direction; however, as the saccade continued into the deceleration phase, the eye was steered correctly, thus partially compensating for the error experienced in the previous trial. As a result, following an error the next saccade improved in the sense that its endpoint exhibited a smaller error (or would have, had the perturbation repeated). Notably, this reduced endpoint error was due to commands that arrived solely during the deceleration period.

To quantify the exact time that the commands correctly changed the eye's trajectory, we analyzed data of each participant separately and looked for the onset time in which $\Delta\dot{H}$ corrected the eye trajectory in the direction of the previous error. The results revealed that error compensation did not begin at saccade initiation (Figure 2.10E, left subplot, mean 24.14 ± 1.12ms, t(36) = 21.54, p =

$7.38X10^{-22}$). Rather, the compensation started 3.67 ± 1.05ms following peak velocity, i.e., slightly after the onset of deceleration (right subplot, Figure 2.10E).

To check the robustness of this result, we re-analyzed the data in Experiments 1 and 2 (n=64 subjects). We measured the change in eye velocity (in the direction of the perturbation) from the first perturbation trial to the next trial only. We found that following experience of an error in trial 1, the correction for that error in trial 2 occurred only during the deceleration period (Figure 2.10F). It was noteworthy that this adaptive response had a larger magnitude than we had observed in Exp. 3. This suggests that when errors are random and reverse direction (as in Exp. 3), there may be a suppression of the adaptive response to error (as compared to errors that are consistently in the same direction)[44].

In summary, following experience of an error, the subsequent primary saccade included small, corrective commands that steered the eyes to reduce the error. However, the expression of these corrective commands did not begin until the onset of the deceleration period (thus violating the coupling required in Model 1). One should always be cautious about interpreting null results such as the lack of adaptation during the acceleration period; however, this result was consistent across all three experiments, bolstering its credibility. Overall, we found that the adaptive response to the experience of a single error was present only during deceleration period of the subsequent saccade.

Discussion

Spontaneous recovery of motor memory is an interesting phenomenon that was correctly predicted by the two-state model of adaptation[7]. Despite the simplicity of the model, however, it has been difficult to identify behavioral correlates of the putative fast and slow states. Neural correlates of the fast and slow processes have been found in the synaptic plasticity mechanisms of single neurons or groups of neurons in the cerebellum[34,45–50]. Correlates of the fast and slow processes have also been noted in distinct

regions of the cerebral cortex and the cerebellum[27,51–63]. Finally, different memory systems (explicit and implicit) have been proposed to contribute to the two putative processes[64,65]. Given these multitude of neural correlates, might it be possible to find behavioral signatures as well? Here, we aimed to identify such correlates in the commands that guide saccadic eye movements.

In Experiments 1 and 2 we observed that following experience of an error, motor commands that guided the subsequent saccades were altered. However, while the acceleration period commands learned relatively little from error and exhibited little forgetting during the set breaks, the deceleration period commands not only adapted with high sensitivity to error, they also suffered significant forgetting during set breaks. These patterns suggested that perhaps the acceleration period commands reflected a slow state of learning, whereas the deceleration period commands reflected a fast state. However, the predictions of this simple model were inconsistent with the data during spontaneous recovery: when adaptation was followed by extinction, the motor commands during the acceleration and deceleration periods both showed spontaneous recovery in the subsequent error clamp block. Thus, the simple two-state model could not account for properties of saccade trajectory during adaptation and spontaneous recovery.

To better understand the experimental results, we considered two models. In Model 1, we imagined that learning was due to a fast and a slow process, but that during a movement some fraction of each process would be expressed during the acceleration period, and the remainder during deceleration. This is akin to a scenario in which learning is limited to a forward model, which corrects the planned movement as it is executed[3]. In Model 2, we imagined two controllers that each had a single timescale of learning, with one controller learning to aim the saccade toward a new location, and another learning to independently modulate commands during the acceleration and deceleration periods. While both models produced good fits to the data, Model 1 could not account for the result that set breaks produced forgetting in only the deceleration period commands. Thus, the modelling

work suggested that learning from error engaged two distinct adaptive processes, providing some independence between the adaption that was expressed during acceleration and deceleration.

To more cleanly test the coupling between acceleration and deceleration periods, we performed Experiment 3, in which the participants experienced a random horizontal error following the conclusion of a vertical saccade. This error induced a change in the commands that guided the subsequent vertical saccade, partially correcting for the error. However, the error-dependent correction was not uniformly expressed throughout the saccade. Rather, the correction took place only via commands that arrived during the deceleration period, providing key support for the idea that the deceleration period commands could adapt independently of acceleration.

There are limitations in our modeling. First, the delineation between Models 1 and 2 is primarily driven by differences in time-based decay, which itself is based on an inability to detect set break decay in acceleration period commands. Second, we encountered a puzzle in Exp. 3 that we could not explain with our models: following experience of an error, the subsequent saccade had deceleration period commands that partially corrected for the previous error. However, there were also changes in the acceleration period commands that moved the eyes in the wrong direction with respect to that error. We currently have no explanation as to why a random sequence of errors should produce such changes in the acceleration period commands of saccades.

Our division of saccade trajectory into acceleration and deceleration was based on our previous observations regarding curvature of saccades during cross-axis adaptation[3]. In that work we found that when a saccade path was divided into four equal segments, the slopes of the first two segments were roughly equal, suggesting a straight line. However, the slopes doubled by the fourth segment, exhibiting a non-linear increase that started at around saccade midpoint, shortly after peak velocity. Results of Exp.

3 in our current report illustrated that while the adaptive response to a single error was present after peak velocity of the saccade, it was missing before this time point.

Taken together, the data suggest that the adaptive response to error is different during the acceleration and deceleration periods: 1) the deceleration period commands learn more from error, and also show a greater forgetting, and 2) adaptation following exposure to a single error specifically engages the deceleration period.

Potential links to neural mechanisms of adaptation

Control of saccade trajectory depends on an internal feedback process that monitors the ongoing movement[66,67], resulting in "steering" of the saccade. For example, in humans it is possible to disrupt a saccade mid-trajectory by using a single pulse of a transcranial magnetic stimulation. Remarkably, that saccade is corrected within the same movement[68]. This internal feedback process likely depends on the integrity of the cerebellum[3,37,38], suggesting that as a saccade is generated by the superior colliculus, the cerebellum monitors and corrects the ongoing motor commands.

Here, our data suggested a degree of independence between the acceleration and deceleration period commands. One possibility is that changes in the acceleration period commands are a form of re-aiming the saccade (Model 2). Re-aiming is present in reach adaptation studies[69–72], raising the possibility that it may also be present in saccade adaptation. If so, we would expect that saccade adaptation would involve changes in how the superior colliculus responds to the visual target. The possibility of target remapping was studied by Quessy et al.[73] and Frens and Van Opstal[74]. They recorded from the superior colliculus and found that during saccade adaptation, locus of activity on the superior colliculus appeared unchanged, thus making remapping unlikely (but see Takeichi et al.[75]). However, Gaymard et al. [76]reported reduced saccade adaptation in patients with lesions in the cerebellar

thalamus. They suggested that the thalamus relayed adaptation-related information from the cerebellum to the cortical oculomotor areas, which can in principle remap the target. Thus, if there is remapping of the target during saccade adaptation, the changes in acceleration period commands might be due to this pathway.

To test whether saccade adaptation involves target re-mapping, future studies can borrow an idea from reach adaptation and manipulate reaction times[69,77]. The idea is that target remapping requires computation time for the brain, and thus by extending reaction times, the brain has a greater potential to re-aim the movement. According to this framework, saccades that have short reaction times, for example express saccades, should exhibit little to no re-aiming, whereas saccades that have long reaction times, for example memory guided saccades, should exhibit significant re-aiming.

Saccades that we studied here are termed "reactive saccades", movements that are triggered in response to sudden appearance of a visual stimulus. Adaptation of reactive saccades relies on the cerebellum[37,78,79]. However, adaptation of voluntary saccades, in which movements scan a scene, relies on both the cerebellum[80] and other structures such as the parietal cortex[81]. It is possible that voluntary saccades in the context of cross-axis adaptation will exhibit a greater amount of re-aiming, and thus produce a larger change in the acceleration period commands.

It seems likely that changes in the deceleration period commands are at least partly due to an adaptive response from the cerebellum. Cerebellar Purkinje cells (P-cells) may be organized into groups based on their preference for direction of visual error[33,48]. This preference for error is expressed via tuning of complex spike probability with respect to the direction of the visual error [33,48,82]. When a saccade concludes and there is a visual error, the result is an increase in the probability of complex spikes for some P-cells, and a decrease in complex spike probability for other P-cells. Both the increase and the decrease in complex spikes promote plasticity in the P-cells: depression of parallel fiber

synapses follows presence of the complex spike, and potentiation follows its absence [34,50,83]. However, the plasticity is greater following presence of a complex spike. Thus, experience of a single error may be followed by differing amounts of learning among various P-cells. This hints that the multiple timescales of adaptation, as expressed in behavior, may be at least partly due to the diverse responses of various P-cell populations to a single error[48].

The idea that there may be separate adaptive controllers for acceleration and deceleration may be relevant to reaching: one controller learns to re-aim the reach, whereas another corrects the movement as it takes place. However, single trial learning in reaching exhibits an error-dependent response that is different than what we found during saccades. In saccades, learning from a single error resulted in corrective motor commands that were expressed primarily during the deceleration period. In reaching, experience of an error produced corrective motor commands that were expressed throughout the subsequent reach[84]. That is, unlike saccades, the single trial response to error for reaching adjusts the motor commands during the entire movement.

Overall, our results demonstrate that the deceleration phase of a saccade exhibits adaptation properties that are distinct from the acceleration phase. This raises the possibility that different neural adaptive control mechanisms contribute to the acceleration and deceleration phases of a single saccade.

Methods

Our goal was to ask whether there were behavioral correlates of the fast and slow adaptive processes within a single movement. In order to do so, we focused on cross-axis saccade adaptation[3,38]: in all experiments, the primary target was placed at 15° from the fixation point at the center of the screen, and upon saccade initiation (on perturbed trials), the target was erased and replaced with a new target at 5° perpendicular to the direction of the original target (Figure 2.1A). Thus, the primary movement

direction and direction of error were perpendicular. This approach has its roots in force field reaching experiments[85], and has the advantage that it disambiguates the primary movement commands from the commands that change in response to error.

Ethics Statement

All subjects gave written informed consent in accordance with policies approved by the Johns Hopkins School of Medicine Institutional Review Board (Protocol Number: NA_00087187) prior to study participation.

General protocol

Participants sat in a chair with their head restrained by a bite-bar made from dental putty (Coltene-Whaledent Inc. Cuyahoga Falls, Ohio, USA). They viewed a computer monitor (AGON 27" 2560X1440, 144Hz) which displayed small square targets (0.25° with 0.1° dark border). They made saccades in response to presentation of the target, and eye movements were recorded from the right eye at 1000 Hz using Eyelink 1000 (S-R Research Ottawa, Ontario, CA).

The basic trial structure is shown in Figure 2.1A. Each trial began with a fixation period of variable duration (randomly sampled from a uniform distribution 250-750ms), during which subjects had to maintain fixation in the center of the screen within a tolerance window of ±2.5°. If they blinked or looked away early, the timer was reset and the trial repeated. After the fixation period, the fixation target disappeared and was replaced by the saccade target. On perturbed trials, immediately after detection of saccade onset the target was jumped 5° perpendicular to the primary saccade direction. Subjects were required to fixate the final target location for 250 ms to complete the trial.

The experiments started with a baseline period without target jumps. During the baseline block, we measured saccade kinematics to targets that were randomly presented on the vertical or horizontal axes, as well as targets along various oblique directions. Vertical saccades were made to a target at (0,+15°). Horizontal saccades were made to targets at (±15,0°). Oblique saccades were made to targets at (±1,15°), (±2,15°), (±3,15°), (±4,15°), or (±5,15°). The oblique saccades served as a control so that we could compare saccade kinematics following adaptation with baseline saccades that had the same endpoint (see Figure 2.4).

In error clamp trials, our objective was to place the target at the location where the saccade would end. To do so, we used linear extrapolation from the state of the eye near saccade end to predict where the eyes would land at the conclusion of the saccade. We measured eye position, velocity, and acceleration when saccade speed fell below 150 deg/sec and used extrapolation to predict gaze location at the time when velocity would cross 0°/sec in the horizontal and vertical directions independently. We then placed the target at that location. To quantify the effectiveness of this approach, we compared the residual error, defined as eye position at saccade end with respect to target, in error clamp trials to error in baseline trials in which the target was not moved. We found that during error clamp trials, errors at saccade endpoint were no different than those observed during baseline saccades (Figure 2.11).

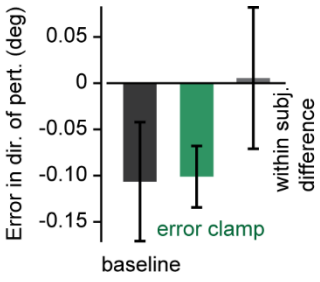


Figure 2.11 Accuracy of error clamp trials. To test whether spontaneous recovery was due to differential decay of multiple learning processes and not to an imperfect implementation of error clamp trials, we calculated the average error in the direction of the original perturbation during the error clamp period of Experiment 2 for each subject and compared it to the average error in the same direction for that same subject during the baseline period (unperturbed trials). We found no difference in error between the two conditions (baseline error: -0.006 ± 0.07° vs. error clamp: -0.10 ± 0.03°, within subject difference: -0.10 ± 0.08°, $t(39) = -1.24$, $p = 0.22$). It should be noted that the visual target occupied a square area of 0.25°, and these error measurements are with respect to the center of that area, so the gaze location is still within the bounds of the visual target under both conditions.

Experiment 1

In this experiment we collected data from 26 subjects, but 2 were removed due to poor calibration that resulted in missing data for ≥15% of trials (final n=24, 22.42 ± 4.0 years old, 11 females). The perturbation was always +5° in the horizontal axis on upward vertical trials (Figure 2.1A). Data from randomly inserted horizontal trials (20% of trials) were not analyzed; these trials were included to introduce uncertainty about the primary saccade location and encourage subjects to maintain fixation for the entire fixation period.

Following a baseline period of 200 trials (80 vertical, 80 oblique, and 40 horizontal), adaptation periods were alternated with error clamp periods, as shown in Fig 1C. Block 1 was an adaptation period of 150 trials (120 vertical trials, 30 horizontal trials), and the subsequent blocks included 100 trials each (80 vertical trials, 20 horizontal trials) until the final error clamp period (150 total trials, 120 vertical trials). In addition, the experiment included set breaks of 30 sec in duration.

The transitions between adaptation and error clamp periods happened in the middle of each block rather than at set breaks to ensure that decay during set breaks did not mask or interfere with early trial-to-trial decay in the error clamp periods. Total experiment length was 1700 trials (1280 vertical trials, 340 horizontal trials, and 80 oblique trials), with 7 adaptation periods and 7 error clamp periods.

Experiment 2

We collected data from n=40 subjects, 26.95 ± 4.86 years old, 10 females. Following a baseline period as in Experiment 1, subjects experienced a 5° perturbation (Figure 2.5C). As before, the perturbation direction was always perpendicular to the primary target direction. However, the subjects were divided

into two equal groups in which the primary target was either upward (vertical) or rightward (horizontal). These two groups were further subdivided equally based on the initial direction of the perturbation (rightward vs. leftward for the vertical group, upward vs. downward for the horizontal group) for a total of four groups with 10 subjects each. The initial perturbation direction was maintained for 525 total trials (420 perturbed trials, 125 perpendicular trials, similar to the horizontal trials in Exp. 1), after which the perturbation switched direction, as shown in Figure 2.5A, lower subplot: that is, the initial perturbation trials were followed by a consistent 5° perturbation in the opposite direction for 50 total trials (40 perturbed trials). The experiment concluded with a block of error clamp trials (125 trials) to assess spontaneous recovery.

Experiment 3

Here we aimed to examine the learning response to a single error. The setup is shown in Figure 2.10A. We collected data from 38 subjects, but one was excluded due to poor calibration that made over 25% of trials unusable (final n=37, 26.08 ± 8.9 years old, 22 females). The experiment consisted of 1350 total trials. The baseline period (180 trials) consisted of 64 trials in which the target was presented along the vertical axis (0,+15°), 36 trials in which the target was presented along the horizontal axis (±15,0°), and 80 trials in which the target was in an oblique direction (as described above). In the perturbation block, rightward and leftward perturbations (±5°) were randomly interleaved with control (no jump) trials to vertical targets (0,+15°) so that every perturbation trial was preceded and followed by at least one control trial to ensure that the measured trial-to-trial changes were truly due to a single error. There was a total of 156 rightward (+5°) and 156 leftward (-5°) target jumps in the perturbation period. We noted a puzzling effect of small changes in the initial horizontal position of the saccade on the acceleration phase of the movement (Figure 2.10D, and Figure 2.11); therefore, we excluded

movements for which the change in horizontal position was greater than 0.5 in either direction. On average, 35 trials (12%) per subject were thus excluded. We divided each saccade into an acceleration phase and a deceleration phase based on peak speed (magnitude of the velocity vector), which was largely dominated by the vertical component, and examined the trial-to-trial change during each movement phase in response to a single error.

Data Analysis

We analyzed our data using in-house code written in MATLAB (The Mathworks, Natick, MA USA), except the repeated measures ANOVAs, which were performed in Rstudio for R using the aov function. Position and velocity data from the eye were filtered off-line using a 3rd-order low-pass Butterworth filter with a cutoff frequency of 200 Hz prior to analysis.

For Experiments 1 and 2, we averaged data in bins of 4 trials and then performed a within-subject repeated measure ANOVA with trial bin and movement phase (acceleration and deceleration) as main effects, including the interaction term, and displacement in the adapted axis as the outcome measure. Learning rates were computed as the mean increase in adaptation during acceleration and deceleration divided by the number of trials (Figure 2.1E). Loss due to set break was computed by aligning displacement data for each subject to set breaks (separately for perturbation and error clamp periods) and then averaging across set breaks to produce a single subject response (Figure 2.1F). We then computed the within subject percent change in displacement due to the set breaks and performed statistics on this measure. Subjects who failed to reach at least 0.25° of adaptation in both phases of the movement prior to the set break were excluded from the percent change analysis (4 subjects thus excluded for Exp. 1 set breaks). The reported changes in horizontal and vertical velocity during the first

set break are the average difference between the last bin prior to the set break and the first bin following the set break during each phase of the movement.

To measure decay patterns during error clamp periods (Figure 2.1G), we averaged the data of each subject within bins of 4 trials each, aligned it to the transition into error clamp from the perturbation period, and computed the average response. We then quantified the within subject percent change in saccade displacement in the error clamp period with respect to the last bin of the preceding perturbation period. We performed a within-subject repeated measure ANOVA for the percent retention with main effects of movement phase and trial bin as well as their interaction (Figure 2.1G).

As a control for Experiment 1, we compared the relative contributions of the acceleration and deceleration phases to total horizontal displacement for baseline (control) oblique saccades and adapted saccades with similar amounts of total horizontal displacement (Figure 2.4). We first performed a 2-way within subject ANOVA with main effects of movement phase and condition (control vs. adapted) including the interaction term. We further calculated the percent contribution of acceleration and deceleration collapsed across the 3 levels of horizontal displacement (1°, 2°, and 3°) and performed paired two-tailed t-tests.

We assessed potential differences in groups for Experiment 2 (Figure 2.6) using a mixed-model ANOVA with error direction (horizontal vs vertical) as the single between subject factor and trial bin number (each bin is 4 trials) and movement phase (acceleration vs. deceleration) as the 2 within subject factors.

We quantified spontaneous recovery by using three periods of 8 trials each (labeled in Figures 2.5B & 2.5C), where t_1 is the end of the initial adaptation period, t_2 is the end of the extinction period, and t_3 is the peak of the spontaneous recovery curve (immediately after the final set break). We defined

spontaneous recovery as the difference between adaptation at t_3 and t_2 divided by the adaptation at t_1 (Figure 2.5E), that is: $[x(t_3) - x(t_2)]/x(t_1)$. Subjects whose adaptation at t_1 in either movement phase was lower than 0.25° were excluded from the spontaneous recovery analysis (5 subjects were thus excluded, final n=35 for spontaneous recovery).

Trial to trial analysis for Experiment 3 relied on the endpoint error that the subjects experienced on any given trial. We calculated error as the final position of the target minus the position of the eye at saccade end and defined errors less than -2.5° as negative errors (H-), and errors of greater than +2.5° as positive errors (H+). We then analyzed the change in horizontal position, displacement, and velocity, from the trial in which the error was experienced to the next trial, as well as the change in vertical velocity (Figures 2.10D & 2.12). To compute the time during the saccade in which the motor commands corrected for the previous error, we flipped the sign of the response to H- errors and combined them with the responses to H+ errors to obtain a single response to error profile for each subject. We then followed the procedures described by [61] to find the timing of the inflection point in the trajectory, resulting in the data shown in Figure 2.10E.

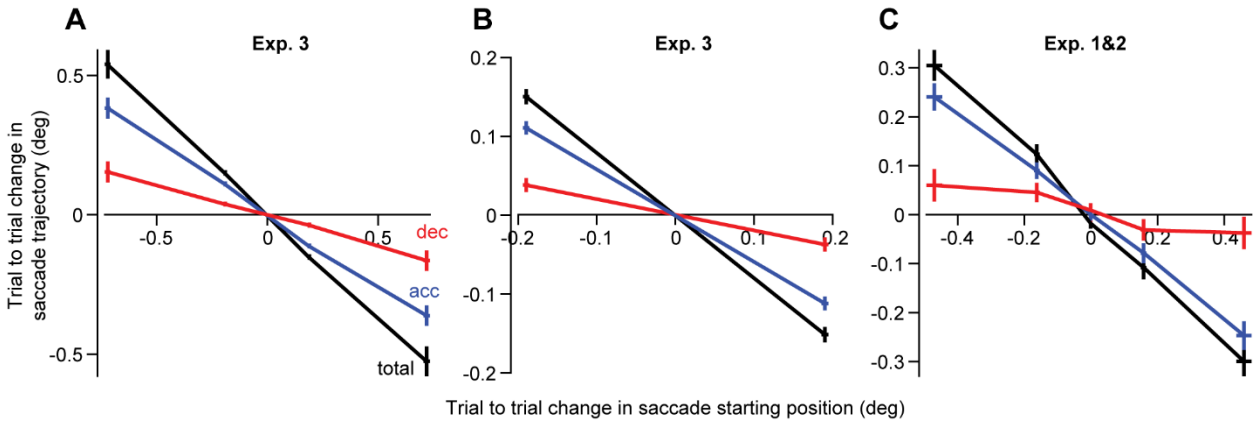


Figure 2.12 Change in horizontal starting position (CHSP) altered saccade displacement, mostly during acceleration. The y-axis quantifies the trial-to-trial change in saccade trajectory during the acceleration and deceleration phases of the saccade. The x-axis shows CHSP of the saccade in trial n with respect to the saccade in the previous trial. **A.** Effect of change in horizontal starting position. Data from Exp. 3. Leftmost bin is CHSP < -0.5°, next is -0.5° < CHSP < 0°, third bin is 0° < CHSP < 0.5°, and the rightmost bin is CHSP > 0.5°. **B.** Close up of middle two bins in part A. **C.** Effect of change in starting position in the baseline periods of Experiments 1 & 2, when there are no errors present

(similar to the mean zero perturbation of Exp. 3). Bins are quintiles of CHSP. As in Experiment 3, there is a strong effect that is mainly expressed during acceleration rather than deceleration. This observation adds further support to the idea that there may be separate controllers that contribute to acceleration and deceleration periods of a saccade.

State-space models

After experience of an error, humans and other animals change their behavior on the subsequent trial. In the absence of error, the adapted behavior decays over time. We used a state-space model to capture this process of error-based learning in our experiments[7,86,87]. The state-space model describes behavior as the summation of underlying hidden states. We represented the internal states via the vector $\boldsymbol{x}$. We investigated the possibility that different parts of the same movement are supported by distinct states, focusing specifically on the acceleration and deceleration components of a single saccade.

One hallmark of adaptation is the presence of spontaneous recovery, a phenomenon in which past learning can be re-expressed in the absence of error. This process requires the existence of multiple timescales of memory, at least one fast and one slow state in the adaptive process[7,43]. In Experiment 2, we found evidence for spontaneous recovery in cross-axis adaptation of saccades. To describe this spontaneous recovery, we first used a standard two-state model. Our initial hypothesis was that the deceleration phase would resemble the model's fast state, and the acceleration phase would resemble the model's slow state. This turned out not to be true, as we found recovery in both the acceleration and deceleration phases of movement, suggesting that both periods have contributions from slow and fast states. Thus, we instead developed two alternate models that could account for these data: Models 1 and 2.

Model 1 was similar to a standard two state model in which there was a single controller that adapted with two states and the sum of these two states affecting behavior. However, a fraction of adaptation (sum of fast and slow states) was expressed early in the movement (acceleration period),

and the remaining fraction was expressed later in the movement (deceleration period). Thus, in this model learning during acceleration and deceleration was derived from a single source.

In Model 2, there were two controllers that contributed to adaptation. One controller produced commands which re-aimed the saccade and contributed to both acceleration and deceleration period commands. A second controller produced commands which independently altered the acceleration and deceleration periods. Here, the idea was that there was a system that learned to aim the saccade, and another system that corrected that movement as it took place. Model 2 was inspired by physiological data regarding control of saccades by the superior colliculus and the cerebellum, which suggested that the cerebellum may play a particularly important role for steering the eyes during the declaration period of a saccade that was initiated by the colliculus. Therefore, in this model, learning during acceleration and deceleration was derived from different sources.

Below, we first describe the elements of our state-space framework common to each model. Then we describe our initial hypothesis, fitting a standard two-state model to the data. Finally, we describe Model 1 and Model 2 each in more detail.

Overview of the state-space model

In a standard state-space model of adaptation, the internal states of the learner change from trial *n* to trial *n*+1. This change is due to learning from error, $e^{(n)}$, and trial-by-trial decay:

$$\boldsymbol{x}^{(n+1)} = A\boldsymbol{x}^{(n)} + be^{(n)} \quad (1)$$

In Eq. (1), x is a vector that contains the state of adaptation. Forgetting is controlled by the retention matrix *A*, a diagonal matrix which enforces that each state independently decays exponentially over trials. The rate of learning is controlled by the error sensitivity vector b. The error sensitivity vector consists of the individual error sensitivities for each internal state. In some cases (see Models 1 and 2 description below) error sensitivity can increase over time, leading to savings[44].

In biological terms, the error is a vector that reflects position of the target with respect to the fovea in the post-saccadic period[48]. This is inferred by the fact that low-intensity stimulation of the superior colliculus at around 80 ms following saccade completion produces complex spikes in the cerebellum[88], and is followed by behavioral changes that resemble saccade adaptation[89,90]. Here, the perturbation was perpendicular to the direction of the main target, and thus we represented error as a scalar quantity that was the distance between saccade endpoint and target position following saccade end.

While we cannot directly measure the internal states x, we can measure their combined effect on the adapted movement:

$$\boldsymbol{y}^{(n)} = C\boldsymbol{x}^{(n)} \tag{2}$$

In the above equation, *C* is a matrix that describes the relationship between the measured behavior and the adaptive states. Here, we describe the behavior, $\boldsymbol{y}$, as a vector that consists of two components: horizontal displacement during acceleration, y_A, and horizontal displacement during deceleration, y_D. The sum of these two displacements yields the total horizontal displacement of the eye, *y*.

Our experiments consisted of a combination of trial conditions. On some trials, a perturbation *r* was applied to the target position. On these trials, the error experienced by the participant was equal to the difference between the perturbation, and the total displacement of the eye. On error clamp trials, movement errors were eliminated. Therefore, the error in Eq. (1) has two possible forms:

$$e^{(n)} = \begin{cases} r^{(n)} - y^{(n)}, & \text{not an error clamp trial} \\ 0, & \text{error clamp trial} \end{cases} \tag{3}$$

Lastly, to model the effect of set breaks (Albert & Shadmehr, 2018), we allowed for decay in the internal states via the matrix *D*:

$$x^{(n+1)} = D^{(n)}(Ax^{(n)} + b^{(n)}e^{(n)}) \tag{4}$$

We allowed decay to differ for each internal state. On normal trials not followed by a set break, the D matrix was set equal to the identity matrix. Therefore, our final state-space model is given by:

$$\begin{aligned} \boldsymbol{x}^{(n+1)} &= D^{(n)}(A\boldsymbol{x}^{(n)} + \boldsymbol{b}e^{(n)}) \\ \boldsymbol{y}^{(n)} &= C\boldsymbol{x}^{(n)} \end{aligned} \tag{5}$$

The form of A, $\boldsymbol{b}$, C, D, and $\boldsymbol{x}$ differ for each model. In the following sections, we describe each of these models in more detail.

The two-state model

We initially tested the possibility that the fast-adaptive state was expressed during deceleration and the slow-adaptive state was expressed during acceleration. Thus, we fit a standard two-state model to our data using the methods initially outlined by[7]. In this model, the total displacement of the eye is described, rather than the individual acceleration and deceleration components. Thus, this model is equivalent to Eqs. (3)-(5) with the exception that y is a scalar (a total displacement) rather than a two-dimensional vector (an acceleration and deceleration component). In this case, the internal state vector $\boldsymbol{x}$ consisted of a slow and fast state: $[x_s\, x_f]^{\mathrm{T}}$. The state vector learned and decayed according to the error sensitivity vector $\boldsymbol{b}$ and the retention matrix A. The vector $\boldsymbol{b}$ was specified by $[b_s\, b_f]^{\mathrm{T}}$. The retention matrix A was specified by a 2 x 2 diagonal matrix whose main diagonal consisted of the retention factors a_s and a_f. Finally, the set break decay matrix D was also a 2 x 2 diagonal matrix whose main diagonal consisted of parameters d_s and d_f which represent the fraction that the slow and fast state decay with the passage of time during a set break (Eq. (4)).

We fit this model to the mean behavior measured in Experiment 2 (shown in Figure 2.5B). In this fit, we enforced the standard two-state dynamics, namely, that the fast state is more sensitivity to error ($b_f \geq b_s$) and the slow state retains its memory more robustly ($a_s \geq a_f$). To fit the model to behavior, we minimized the squared error between the model and the average data across all participants in

Experiment 2. The fast and slow states predicted by the model are shown in Fig 2.5C. Note that these states did not resemble the deceleration and acceleration commands shown in Fig 2.5B.

Model 1

In our first model, we imagined that the adaptation expressed during acceleration and deceleration was derived from a single source. As time elapsed during a movement, a fraction of the adapted motor commands was expressed during the beginning phase of the movement (i.e., acceleration) and the rest of adaptation was expressed during the later phase of the movement (i.e., deceleration). Therefore, Model 1 supposed that y_A and y_D were derived from the same states and each differentially expressed some fraction of the total adaptation. In this case, Eq. (2) takes the following form:

$$y_A = p(x_s + x_f)$$
$$y_D = (1-p)(x_s + x_f) \quad (6)$$

Here the variable p represents the fraction of total adaptation expressed during the acceleration phase. By extension, the quantity $1-p$ represents the fraction expressed during deceleration. Adaptation from both phases is derived from the same slow and fast states, denoted x_s and x_f, respectively.

The slow and fast states learn and decay (as in Eq. 1) using the standard form of the error sensitivity vector $\boldsymbol{b}$ and retention matrix A. The vector $\boldsymbol{b}$ consists of the error sensitivity for the slow, b_s, and fast, b_f states of learning. The retention matrix A is a 2 x 2 diagonal matrix whose main diagonal consists of the retention factor for the slow, a_s, and fast, a_f, states of learning.

Critically, because Experiments 1 and 2 involved long and sometimes repeated (Exp. 1) exposure to the perturbation, we allowed error sensitivity to increase over time[44]. Without this, the state-space model cannot exhibit a key aspect of adaptation: savings, i.e., a faster and more complete learning with each re-exposure to the perturbation. Thus, in the model, b_s and b_f both start at initial values of $b_{s,0}$ and $b_{f,0}$ respectively, and increase by β_s and β_f on each perturbation trial (i.e., error sensitivity increased only

when an error was observed, not on error clamp trials). Note that because b is specific to a given error[44], b_s and b_f were reset in Experiment 2 back to $b_{s,0}$ and $b_{f,0}$ when the perturbation switched sign.

We enforced the conventional two-state dynamics, namely, that the fast state is more sensitive to error ($b_{f,0} \geq b_{s,0}$) and the slow state retains its memory more robustly ($a_s \geq a_f$). Finally, the set break decay matrix D is also a 2 x 2 diagonal matrix whose main diagonal consists of parameters d_s and d_f which represent the fraction that the slow and fast state decay with the passage of time during a set break (Eq. (4)).

In summary, Model 1 consists of 9 parameters: {a_s, a_f, $b_{s,0}$, $b_{f,0}$, d_s, d_f, p, β_s, β_f}. We will describe the process by which we fit the model to behavior in text below.

Model 2

In this model, we imagined two controllers that each had a single timescale of learning. One controller learned to aim the saccade toward a new location, and another learned to independently modulate commands during the acceleration and deceleration periods. The aiming controller re-aimed during acceleration by the proportion p and deceleration by the proportion $1 - p$:

$$y_{acc}^{(n)} = p x_{aim}^{(n)} + x_{acc}^{(n)}$$
$$y_{dec}^{(n)} = (1-p) x_{aim}^{(n)} + x_{dec}^{(n)} \quad (7)$$

The states changed following experience of error:

$$x_{aim}^{(n+1)} = a_{aim} x_{aim}^{(n)} + b_{aim} e^{(n)}$$
$$x_{acc}^{(n+1)} = a_{acc} x_{acc}^{(n)} + b_{acc} e^{(n)}$$
$$x_{dec}^{(n+1)} = a_{dec} x_{dec}^{(n)} + b_{dec} e^{(n)} \quad (8)$$

Therefore, the internal state vector $\boldsymbol{x}$ consisted of $[x_{aim}\ x_{acc}\ x_{dec}]^T$. The state vector learned and decayed according to the error sensitivity vector $\boldsymbol{b}$ and retention matrix A. The vector $\boldsymbol{b}$ was specified by the vector $[b_{aim}\ b_{acc}\ b_{dec}]^T$. The retention matrix A was a 3 x 3 diagonal matrix whose main diagonal

consisted of the retention factors a_{aim}, a_{acc}, and a_{dec}. Finally, each state decayed independently during a set break according the 3 x 3 diagonal matrix *D*, whose main diagonal consisted of the time-decay parameters d_{aim}, d_{acc}, d_{dec}. Similar to Model 1, to permit savings we allowed error sensitivity to increase over time. To do this, ***b*** started at initial values $\{b_{aim,0}, b_{acc,0}, b_{dec,0}\}$ and increased on each perturbation trial. As in Model 1, ***b*** was reset to its initial values when the perturbation switched sign in Experiment 2. To allow error sensitivity to increase over time, we multiplied the initial error sensitivity vector element-wise by scaling factor determined by $\{\beta_{aim}, \beta_{acc,} \beta_{dec}\}$. Given the high dimensionality of this parameter set, we conducted a set of model comparisons to determine which, if any, of the trial-based retention (*a*), time-based retention (*d*), and error-based learning parameters (*b* and β) were common across the various states.

To compare these model variants, we fit each to participant measured data in Experiments 1 and 2 by minimizing the following cost function:

$$\theta_{fit} = \underset{\theta}{argmin} \sum_{n=1}^{N} (y_A^{(n)} - \hat{y}_A^{(n)})^2 + (y_D^{(n)} - \hat{y}_D^{(n)})^2 \quad (9)$$

Here, $\hat{y}_A$ and $\hat{y}_D$ refer to the amount of adaptation expressed during acceleration and deceleration predicted by each model (Eq. (7)). Therefore, rather than fit the model to the total displacement of the eye, we fit the model to the individual acceleration and deceleration commands observed on each trial. To do this, we performed 100 iterations of *fmincon* in MATLAB R2018a (subject to the inequality constraints describing the conventional two-state dynamics), each time varying the initial parameter guess. We selected the parameter set across the 100 iterations that minimized squared error.

After fitting each model variant, we used the model's RMSE, the number of observations for each participant, and the number of free parameters to compute the BIC for each model. We did this for each participant, and then added each BIC across participants to calculate the total BIC for each model. This model comparison revealed that the most parsimonious model variant that best explained the

behavior in Experiments 1 and 2 required only the following 9 parameters: {a_{aim} a_{acc} a_{dec} $b_{aim,0}$ $b_{acc,0}$ $b_{dec,0}$ d_{dec} b p}. The b represents that all 3 states increased their error sensitivity at the same rate.

Behavioral and statistical comparison of Models 1 and 2

In Figure 2.7 we investigated whether Models 1 and 2 could account for various aspects of behavior measured in Experiments 1 and 2. We compared the models in two different ways. First, we focused on how each accounted for key behavioral findings, such as the magnitude of decay after a set break. Second, we compared each model statistically via maximum likelihood (Figure 2.9A).

To compare the behavioral phenomena predicted by Models 1 and 2, we identified the model parameters that best fit the measured behavior in Experiments 1 and 2 (Figure 2.7A) by minimizing the following cost function:

$$\theta_{fit} = \underset{\theta}{argmin} \sum_{n=1}^{N} (y_{A,E_1}^{(n)} - \hat{y}_{A,E_1}^{(n)})^2 + (y_{D,E_1}^{(n)} - \hat{y}_{D,E_1}^{(n)})^2 + (y_{A,E_2}^{(n)} - \hat{y}_{A,E_2}^{(n)})^2 + (y_{D,E_2}^{(n)} - \hat{y}_{D,E_2}^{(n)})^2 \quad (9)$$

Here, the y terms refer to either the mean acceleration and deceleration measured in Experiment 1 or Experiment 2 (denoted with the subscripts E_1 and E_2 respectively). The $\hat{y}$ terms denote the behavior predicted by either Model 1 or Model 2. We chose this cost function so as to maximize the robustness of our least-squares fitting technique, which is prone to errant predictions when measured behaviors are described by multiple hidden components[91]. Specifically, we fit to Experiments 1 and 2 simultaneously to ensure generalization of the underlying parameter set. We also fit to the mean behavior across participants (all participants that were adapted to horizontal errors), to reduce the impact of behavioral noise sources on the fitting process. And finally, we fit not to the total displacement, but to the individual acceleration and deceleration components to further constrain the model fit. Under these conditions, we expect our least-squares algorithm to perform similarly to other maximum likelihood techniques[91]. To further assess our ability to accurately recover model parameters, we also conducted a parameter recovery analysis (Figure 2.8).

This minimization was performed using *fmincon* in MATLAB R2018a. To ensure that the global minimum of Eq. (9) was identified, we performed 100 iterations of *fmincon*, each with a different randomly specified initial condition. The parameter set associated with the smallest squared error was selected. We then used this parameter set to simulate behavior in Experiments 1 and 2 (Figure 2.7). The parameter sets for Models 1 and 2 are reported in Table 1.

We used bootstrapping to identify confidence intervals for each parameter in Models 1 and 2. To do this, we randomly sampled participants from Experiments 1 and 2, with replacement. For each random sample, we computed the mean behavior, and fit Models 1 and 2 to that mean behavior by minimizing Eq. (9). We repeated this process 10,000 times, and selected the interior 95% of each parameter distribution. These intervals are also reported in Table 1.

The primary disagreement between Models 1 and 2 was their predictions regarding time-based decay after a set break. These predictions are quantified in Figure 2.7D. To quantify the magnitude of decay predicted by the model during acceleration and deceleration, we analyzed individual participant data. For each participant, we calculated the total set break decay predicted by Models 1 and 2, using the best fit parameters for that participant. For each participant, we calculated the predicted model decay after each set break, and then averaged across set breaks. In Figure 2.7D, we combined participants from Experiments 1 and 2 when quantifying set break decay during perturbation periods. However, only Experiment 1 was used in our analysis of error clamp period set-breaks because the error clamp period in Experiment 2 was during the period of spontaneous recovery.

We also statistically compared Models 1 and 2 via maximum likelihood estimation. We fit Model 1 and Model 2 to each participant's behavior in Experiments 1 and 2 by minimizing the cost function in Eq. (8). To do this, we performed 100 iterations of *fmincon* in MATLAB R2018a (subject to the inequality constraints describing the conventional two-state dynamics), each time varying the initial parameter guess. We selected the parameter set across the 100 iterations that minimized squared error. For each

participant, we used the model's RMSE and total trial count to calculate the log-likelihood for each fit. In Figure 2.9A, we compared the log-likelihood for Models 1 and 2. In addition, we also performed a model recovery analysis (Figure 2.9B). This analysis is detailed in the figure caption.

Chapter 3: Cross-Axis Saccade Adaptation in Marmosets

Introduction

It has long been theorized that the purkinje-cells (P-cells) of the oculomotor vermis (OMV) of the cerebellum are essential to saccade accuracy and saccade adaptation [20,33,38,92–96]. However, the exact relationship between the activity of these cells and saccade adaptation remains unclear. Here, we present evidence in support of the role of P-cells in the OMV in both saccadic execution and saccade adaptation.

The Marr-Ito-Albus hypothesis states that the complex spikes (CS) of cerebellar P-cells serve as the error signal for cerebellar-dependent saccade adaptation via long-term depression (LTD) and long-term potentiation (LTP) of the simple spikes (SS) in subsequent movements [94–96]. In order for this to be true, CS firing must be sensitive to visual errors, but the data are mixed. Catz et al. found no evidence that CS encoded endpoint errors during saccade adaptation [97], but Soetedjo et al. found that CS firing rates were highest when aligned to saccade offset, i.e. the onset of the visual error [28]. Likewise, Soetedjo and Fuchs found that while the probability of a CS was not sensitive to the magnitude of endpoint error, it was sensitive to the direction [98]. Similarly, slightly over half of P-cells exhibited SS changes correlated with adaptation in a gain-down task, whereas others did not [99]. Other studies, however, have found evidence that the presence of a CS in one trial leads to a change in both SS and behavior on the subsequent trial [34,83]. Further, another study found errors in CS-on, the preferred error direction of a P-cell, produced greater depression of SS over trials than errors in CS-off (CS-on+180^{o}) did potentiation [50]. Finally, others have found the probability of a CS was related to learning rate during saccade adaptation [98], and the behavioral change caused by a CS is in the direction of CS-on of that P-cell regardless of the presence, absence, or direction of error [34].

In this study, we recorded from P-cells of the OMV in marmosets during a novel cross-axis saccade adaptation experiment. Cross-axis adaptation rather than in-axis (gain up or gain down) has the advantage that the adapted response is perpendicular to the primary movement, making it easier to isolate and analyze. In a previous study in human subjects, we found evidence that there may be a shared as well as separate controllers contributing to cross-axis saccade adaptation, with distinct contributions expressed during the acceleration and deceleration periods of the saccade, and speculated that the distinct controllers may be supported by distinct subpopulations of P-cells in the OMV, one that experienced errors in CS-on and one that experienced errors in CS-off [100]. Here, we aimed to test that hypothesis in a marmoset model while recording from P-cells in the OMV. Our results indicate that these P-cells are indeed important for this saccade adaptation and showed evidence of distinct changes in SS modulation and contributions to adaptation of CS-on and CS-off subpopulations.

Methods

Animals

We collected and analyzed data from 2 healthy adult common marmosets (*Callithrix jacchus*), one male (R 355g, X years old), one female (M 342g, Y years old). Both animals were born and raised in the colony Xiaoqin Wang has maintained at the Johns Hopkins School of Medicine since 1996. Animal protocols and procedures were reviewed and approved by the Johns Hopkins University Animal Care and Use Committee in compliance with the guidelines of the United States Institutes of Health. Animals were surgically implanted and trained to make saccades to visual targets on an LCD screen (INFO) to earn a reward of an apple sauce lab diet mixture as described previously [82] while binocular eye movements were recorded using an EyeLink-1000 eye tracking system (SR Research).

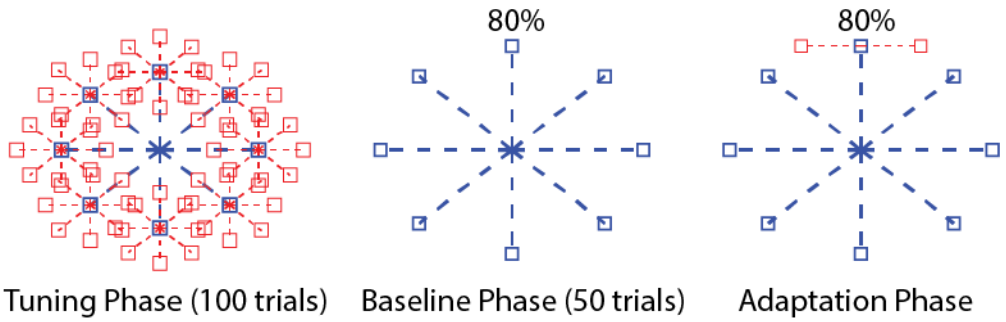


Figure 3.1 Experiment structure. The experiment started with 100 trials of both primary (blue) and secondary (red) saccades to assess the error-response (CS tuning) curve of any recorded P-cells. After that, was a 50-trial baseline period with no secondary targets and 80% of trials in the upward direction. The remaining 20% were randomly distributed among the other 7 directions. Finally, in the adaptation phase, secondary targets were either rightward or leftward of the primary target only on the upward vertical trials, which were 80% of all trials.

Behavioral Protocol

Each trial started with the animal fixating the target (0.5^{o} per side square) at a central "neutral" point on the screen for a variable time drawn from a random uniform distribution of 200ms to 500ms (need to check these exact numbers). Then, the target jumped to its primary location at distance of 5.5^{o} from the fixation point as determined by the experimental protocol. The animal then needed to make a saccade toward the target. On perturbation trials, the target was jumped 2.5^{o} as soon as saccade onset was detected, and the animal needed to make a secondary (corrective) saccade to the target and fixate it to complete the trial and receive reward. On other, non-perturbation trials, the target remained in its primary location, and the animal only needed to make a primary saccade and fixate the target to complete the trial. The experiment consisted of 3 distinct phases, in order: 1. Complex Spike Tuning (CST) 2. Baseline 3. Adaptation (Figure 3.1). The experiment began with the CST phase, which lasted for 100 trials and during which primary and secondary target locations were randomly and evenly distributed among 8 directions (up, down, right, left, and the principal diagonals) for a total of 64 possible combinations (Figure 3.1, left). This was to generate as many post-saccadic error signals in a range of directions as possible in order to assess the error preference/complex spike tuning of recorded P-cells. Following completion of the CST phase, the Baseline phase began, which lasted for 50 trials and during which 80% of primary targets were in the upward (90^{o} from right horizontal) direction with the

remaining 20% randomly distributed among the other 7 directions (Figure 3.1, middle). There were no secondary targets during this phase. Finally, upon completion of the baseline phase, the experiment entered the Adaptation phase. The distribution of primary targets was identical to the baseline phase; however, now, perturbation trials were introduced. These only occurred in the 80% of trials with an upward primary saccade direction, and the secondary targets were either leftward or rightward of the primary target such that the post-saccadic error, secondary saccade, and adaptation would all be perpendicular to the primary saccade direction (Figure 3.1, right). The experiment concluded when the animal began disengaging from the task or after the animal had been in the chair for 5-6 hours.

Neurophysiology

We recorded acutely from Purkinje-cells (P-cells) of the cerebellar oculomotor vermis using either 7 fiber (heptode) metal core (platinum/tungsten 95/05) electrodes (Thomas Recording) or 64 contact high-density silicon probes (Cambridge Neurotech). We connected the electrode to either a 32- or 64-channel (respectively) head stage amplifier and digitizer (Intan Technologies) and then connected the head stage to a communication system (RHD2000, Intan Technologies). Data were sampled at 30 kHz and band-pass filtered (2.5-7.6 Hz). We computed a common average reference signal (median of all simultaneously recorded channels, computer at 30 kHz) and subtracted this signal from all channels. We interfaced with the RHD2000 system and recorded signals using OpenEphys[101], an open-source extracellular electrophysiology data acquisition software.

Spike Sorting and Data Processing

We performed spike sorting and P-cell identification using p-sort, an open-source software developed previously in our lab and described previously [102], for the heptode recordings and Kilosort and Phi [103] for the high-density probe recordings. We included P-cells if and only if they were present

during the first recording of the day because the first recording always contained the CS-tuning and baseline phases of the experiment. For the simple spike analysis, we included only P-cells for which we could verify simple spikes (SS) and complex spikes (CS) from the same cell (i.e. the CS suppressed the SS), but for the complex spike analysis, we included all CS signals that were present in the first recording. This approach yielded in 68 P-cells for the SS analysis and 114 P-cells for the CS analysis.
We used MATLAB (r2021b The Mathworks) to process and analyze behavioral and neurophysiological data as well as align their timeseries. Data were aligned to either saccade onset, saccade peak speed (vmax), saccade offset, or the visual event (target appearance) that prompted the saccade.

Data analysis

Offline data processing and analysis were performed in MATLAB, with the exception of the repeated measures ANOVAs, which were performed using Rstudio for R after formatting the data in MATLAB. The first step was the identify all the saccades made during the experiment. Saccades were identified using a filtered speed trace (Butterworth, 3rd order, cut-off frequency of 50Hz) and a speed threshold of 75^{o}/sec and a "peak height" of at least 50^{o}/sec. Saccade onset and offset were identified using a 20^{o}/sec threshold where possible and a 50^{o}/sec threshold if needed. Once all saccades were identified, each saccade was assigned 1 of 10 tags depending on its characteristics (see Table 1: Saccade Tag Definitions). Further, saccades were separated into 8 bins based on their movement direction. This was done by calculating the angle between the gaze location when the target appeared and the location of the target. Thus, saccades were subdivided by tag and movement direction for analysis.

The main behavioral outcome measures were the amount of adaption and the proportion of that adaptation that was present during the acceleration and deceleration phases. We defined adaptation as the amount horizontal displacement in the direction of the error during the upward Tag 1

(successful primary) saccades. We considered Tag 6 (back to center) saccades as controls since they were task-relevant primary saccades of similar magnitude.

We analyzed the learning curves using two different binning methods. In both methods, however, we binned the baseline period separately from the adaptation period to ensure the transition between phases did not occur within a bin but rather across bins. First, we binned trials using a traditional method where we simply chose a bin size and computed however-many bins we had saccades for each day. However, because the number of trials, and therefore, of saccades in the adaptation period differed from day to day, this resulted in a large variation in the number of bins per day and a decreasing number of days in each bin (and reduced statistical power) as the number of bins increased. In order to counteract this problem and still use all of the data we collected, we also binned saccades by a percentage of the total number of saccades completed that day. In this method, we chose the number of bins and then calculated the number of saccades per bin based on the number of saccades recorded that day. For the behavior data, we chose 4 bins for the baseline period, and either 16 bins for the adaptation period.

The outcome measures for the neurophysiology data were the CS-tuning directions and distribution for the recorded P-cells, the SS modulation during upward Tag 1 saccades and the CS modulation following upward Tag 1 saccades (when the animal experienced the visual error). We considered Tag 1 saccades in other directions as a control for the SS analysis.

We identified P-cells as simultaneous SS and CS signals on the same channel in which the CS suppressed the SS. We then calculated the preferred CS direction (CS-on) by calculating the error direction (among 8 bins) that produced the highest probability of a complex spike in the 200ms following the error.

We divided the population of our recorded P-cells into subpopulations based on the relationship between their CS-on direction and the direction of the error the animal experienced (jump direction)

while that P-cell was recorded. We categorized P-cells with an absolute value of the difference between CS-on and jump direction ≤ 90^{o} as "CS-on cells", and P-cells in which the difference between CS-on and jump direction was greater than ± 90^{o} as "CS-off cells." Finally, we recombined these subpopulations to calculate the total population response by subtracting the activity of the CS-off cells from that of the CS-on cells.

We determined spike modulations by baseline subtracting each cell, using its firing rate during saccades of the same tag in the same direction during the CS-tuning and baseline phases (prior to adaptation onset); further, we also subtracted the mean firing rate of that cell during the fixation period (240 to 50 ms prior to the alignment event) during each trial bin in order to specifically target the saccade-related modulation. We performed this modulation analysis on separately on the CS-on cells and the CS-off cells as well as for the population.

We measured synchrony via a synchrony index calculated by dividing the joint probability of both cells of a simultaneously recorded pair each firing a spike within 1 ms of each other by the chance level of a synchronous spike. We calculated chance by shuffling the trials and calculating the shuffled joint probability. In addition, we used the CS from both P-cells in each pair to calculate a "pair CS-on" and divided the pairs into 2 subpopulations, one that experienced errors near their preferred error direction (CS-on Pairs) and one that experienced errors far from their preferred error direction (CS-off Pairs).

Statistics

We assessed learning by performing a repeated-measures analysis of variance (RMANOVA) for each animal on the amount of adaptation with saccade bin as the main factor. We then performed post-hoc single sample student's t-tests on the amount of adaptation in the final adaptation bin each day for

both animals individually and compared adaptation between animals using Walsh's test for unequal sample sizes.

We compared the amount of adaptation present in the acceleration and deceleration phases for each animal using a RMANOVA with saccade bin and movement phase (acc vs. dec) as the main factors and including the interaction term. Further, we performed post-hoc single sample t-tests for the amount of adaptation in each phase in the final saccade bin of the day separately for acceleration and deceleration. Furthermore, we compared the amount of adaptation present in the acceleration and deceleration phases for each animal using a paired-sample t-test. Finally, we compared the amount of adaptation in each phase of the movement between animals using Welch's test for unequal sample sizes. We computed the standard error of the mean for the comparisons between animals by bootstrapping with 10,000 repetitions.

We assessed SS and CS modulation related to upward Tag 1 saccades using the mean firing rate during a specified time window (during saccade for SS and 1 to 200 ms after saccade offset for CS) with timepoints of baseline, early adaptation (first half of adaptation period), and late adaptation (second half of adaptation period). We assessed changes in SS and CS modulation via RMANOVAs with timepoint as the main factor. We performed this analysis on both the CS-on and CS-off subpopulations. Additionally, we performed t-tests on the within-P-cell change in SS modulation from baseline to late adaptation and in CS from early adaptation to late adaptation.

Because we calculated the population response by subtracting the CS-off subpopulation mean from the CS-on subpopulation mean, we used bootstrapping with 10,000 bootstrapped samples to test a difference in means for the SS modulation of the population from baseline to late adaptation as well as a difference in means for the CS modulation of the population from early adaptation to late adaptation.

Finally, we wanted to test for any changes in SS or CS synchrony in the CS-on and CS-off subpopulations; however, the data were too sparse for yield reliable results from statistical hypothesis tests due to the high percentage of missing values (24% and 55% for the CS-on and CS-off subpopulations respectively).

Results

Behavior

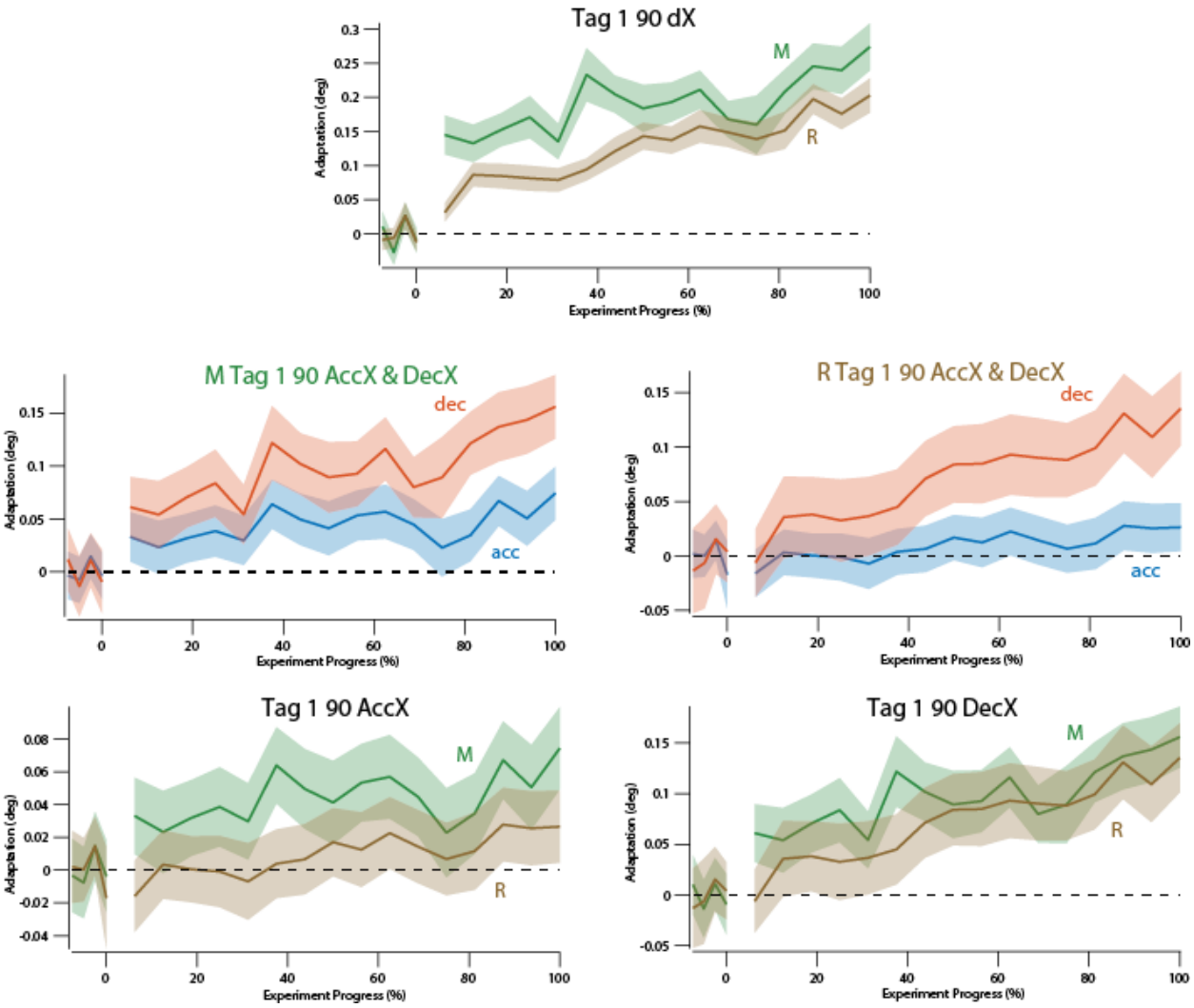


Figure 3.2 Behavioral Results. Top: Amount of adaptation for Monkey M (green) and Monkey R (brown). Adaptation is the amount of horizontal displacement in the direction of the target jump during the upward primary saccades. X-axis for plots is the percent of saccades completed for the day. Both animals showed significant adaptation to the target jump. Middle Left: Amount of adaptation expressed during acceleration (blue) and deceleration (orange) for Monkey M. Adaptation during deceleration is greater than during acceleration. Middle

Right: Adaptation expressed during acceleration and deceleration for Monkey R. Much greater adaptation during deceleration than acceleration. Bottom Left: Comparison of acceleration phase for the two monkeys. Monkey M appears to have a greater adaptation level than Monkey R, although this difference was not statistically significant. Bottom Right: Comparison of deceleration for the two monkeys. No difference.

Both animals showed significant adaptation during upward Tag 1 saccades as the experiment progressed (Figure 3.2, top; Monkey M, RMANOVA Main effect of bin: $F(19,1501) = 6.73$, $p<0.001$; Monkey R, RMANOVA main effect of bin: $F(19,760) = 12.91$, $p<0.001$). Monkey M adapted rapidly early on with a sharp jump in adaptation from baseline in the first bin and reached a some what higher final level of adaptation than Monkey R (0.16 ± 0.03^o, $t(79) = 4.69$, $p<0.001$ vs 0.11 ± 0.05^o, $t(40) = 2.08$, $p=0.04$, respectively), who adapted more evenly throughout the experiment (Figure 3.2 Top, green vs. brown curves), although this difference did not reach statistical significance ($t(72.64) = 0.75$, $p=0.45$).

Examining the amount of adaptation expressed during the acceleration and deceleration phases confirmed the main effect of bin for both animals (Figure 3.2, middle row; M: $F(19,1501)=6.52$, $p<0.001$; R: $F(19,760)=12.02$, $p<0.001$); however, only monkey R showed a significant main effect of movement phase (M: $F(1,79)=3.75$, $p=0.056$; R: $F(1,40)=6.56$,$p=0.01$), as can be seen in the greater nearness and similarity of the acceleration and deceleration adaptation curves for Monkey M and for Monkey R (Figure 3.2, middle row, left vs right panels). Crucially, and in agreement with our prior results in human subjects, both animals showed a significant interaction of bin and movement phase, indicating a different slope across bins between phases (M: $F(19,1501)=6.52$, $p<0.001$; R: $F(19,760)=10.09$, $p<0.001$). We therefore examined the adaptation expressed during each phase in more detail. Both animals expressed significant levels of adaptation during the deceleration phase (Figure 3.2, middle row, orange curves; M: 0.14 ± 0.03^o, $t(79)=4.60$, $p<0.001$; R: 0.13 ± 0.03^o, $t(40)=3.94$, $p<0.001$). However, only Monkey M expressed significant adaptation during the acceleration phase (Figure 3.2, middle row, blue curves; M: 0.07 ± 0.02^o, $t(79)=2.93$, $p=0.004$ vs. R: 0.03 ± 0.02^o, $t(40)=1.15$, $p=0.25$). Importantly, both animals expressed more adaptation during the deceleration phase than the acceleration phase (within-animal-and-day difference M: 0.06 ± 0.01^o $t(79)=4.58$, $p<0.001$; R: 0.11 ± 0.02^o, $t(40)=5.20$, $p<0.001$).

There were no significant differences between animals in the amount of adaptation expressed during the two phases of the movement, however (Figure 3.2, bottom row; Acc: 0.05 ± 0.03°, t(113.82) = 1.4, p=0.15; Dec: 0.004 ± 0.04°, t(96.78) = 0.09, p=0.93).

Neurophysiology

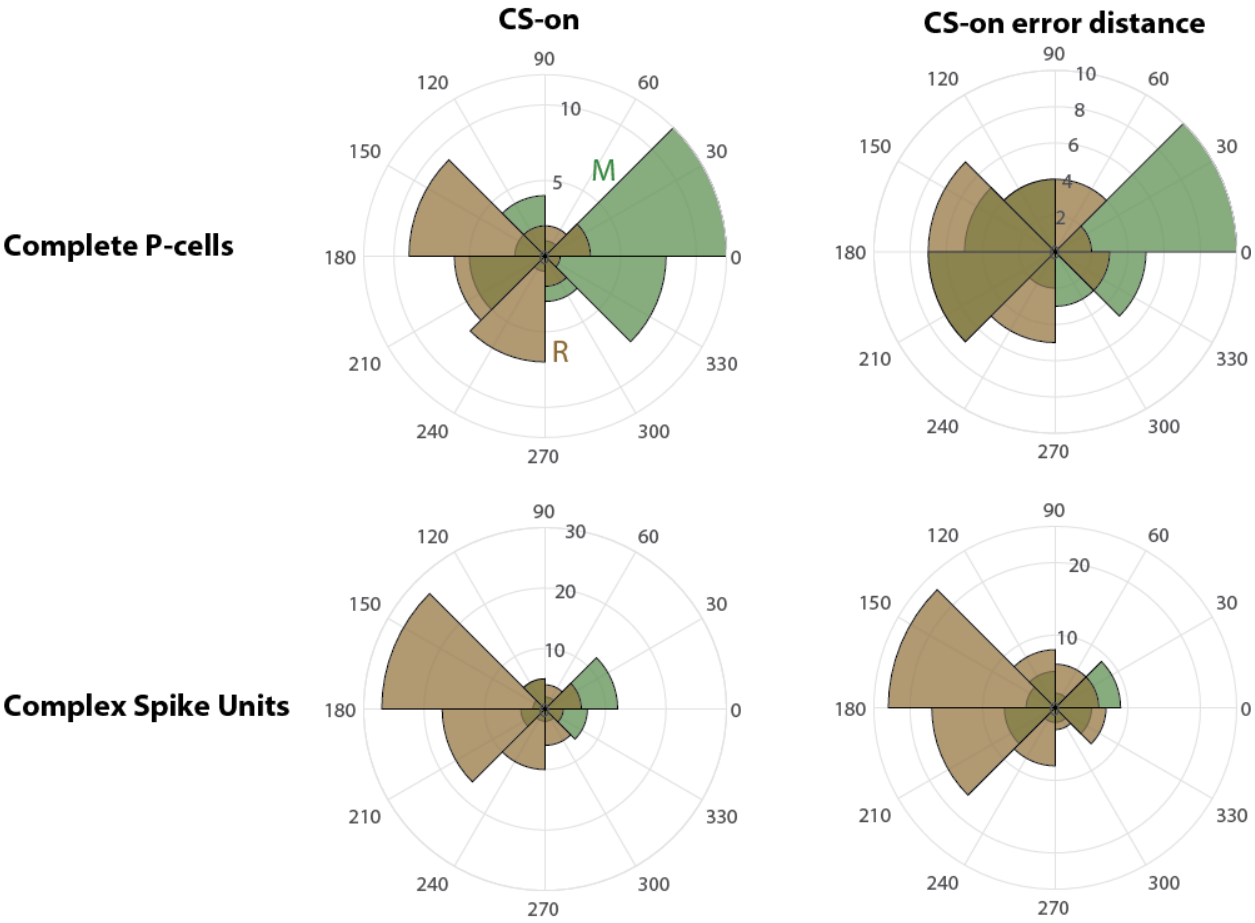


Figure 3.3. CS-on distributions. Left column: Distribution of preferred error directions (CS-on) for the 68 P-cells in our dataset. Green represents P-cells from Monkey M, and brown shows P-cells from Monkey R. While both animals had a range of preferred error directions, the P-cells from M tended to have more rightward preferred errors, and the P-cells from R tended to have more leftward preferred errors. Right column: Distribution of the difference between CS-on and target jump direction. Zero means the target jump (and therefore the visual error) was in CS-on of the cell(s) we recorded that day. Both animals provided cells in both CS-on and CS-off (CS-on+180°). Top row: Complete Purkinje cells (both SS and CS with CS suppression of SS). Bottom row: CS units (with or without SS).

The first step of our analysis of the neurophysiology data was to identify P-cells and calculate their preferred error direction CS-on (see Methods). Then, for each P-cell, we compared the direction of the target jump on the day it was recorded to CS-on for that cell in order to subdivide our P-cells into a subpopulation that experienced errors in/near its preferred error direction (CS-on Cells) and a subpopulation that experienced errors far from/opposite its preferred error direction (CS-off Cells; see Methods). The CS-on directions for the P-cells we recorded were well-distributed around the error space, although most P-cells had generally horizontal CS-on directions (Figure 3.3, left). Moreover, Monkey M had many P-cells with a rightward CS-on, whereas Monkey R had more P-cells with a leftward CS-on. However, both animals experienced errors in both directions, and so both animals provided P-cells for both the CS-on and CS-off subpopulations (Figure 3.3, right). In total, we recorded 40 complex spike units and 27 complete P-cells in the CS-on subpopulation and 74 complex spike units and 41 complete P-cells in the CS-off subpopulation for a total of 114 CS units and 68 complete P-cells (Table 3.1).

	Complete P-cell	CS-only	Total
CS-on Subpopulation	27	13	40
CS-off Subpopulation	41	33	74
Population	68	46	114

Table 3.1 Recorded units and subpopulations

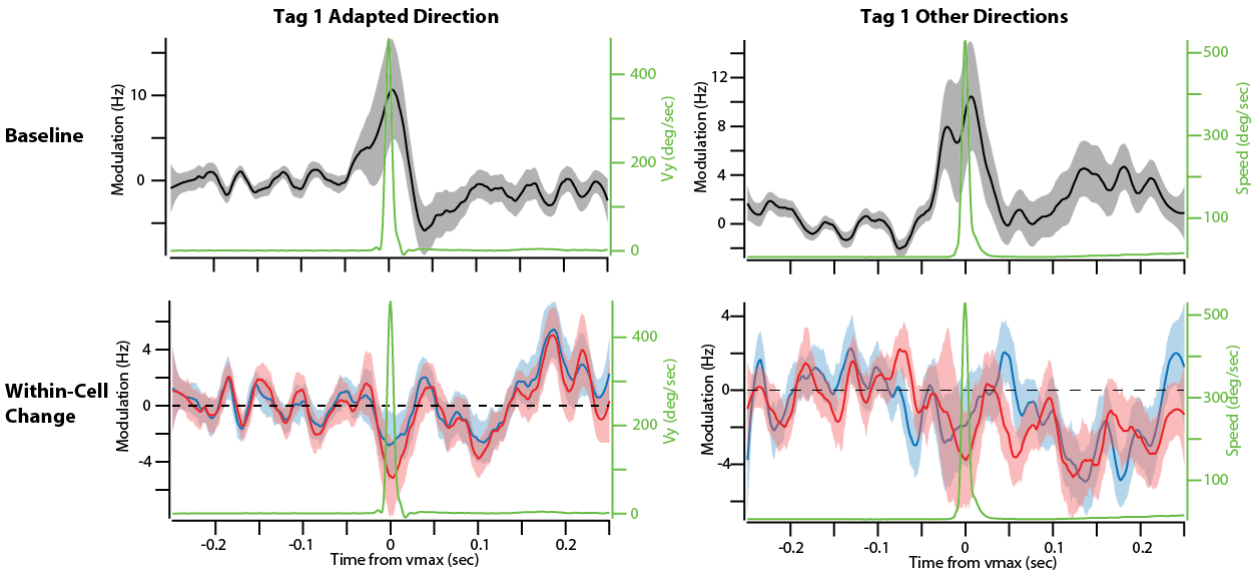


Figure 3.4. SS Modulation of the CS-on subpopulation. Top row is SS modulation during baseline period. Bottom row is the within cell change from baseline. Blue curve is early adaptation, and the red line is late adaptation. Left y-axes show modulation in Hz. Right y-axes show Vy (green curve) in the left column and speed in the right column. Data are aligned to peak speed (x-axes). Left column shows responses during upward Tag 1 (successful primary) saccades. There is a significant reduction in the saccade related burst in late adaptation. Right column shows responses during Tag 1 saccades in all other (non-adapted) directions. There are no significant within-cell changes.

We first analyzed the within-cell change in the saccade-related SS modulation from baseline to early and late adaptation for the CS-on subpopulation (Figure 3.4). At baseline, CS-on cells showed an SS burst beginning just prior to saccade onset and terminating just after saccade offset; this was true for both upward Tag 1 saccades and downward Tag 6 saccades (Figure 3.4, top row). Now, we know that: 1. CS suppress SS and cause LTD 2. Cells in this subpopulation are experiencing a post-saccadic foveal error following upward Tag 1 saccades error due to the intra-saccadic target jump (secondary target) and that error is in/near their preferred error direction. Therefore, we expected a reduction in the saccade related SS burst for Tag 1 saccades in this subpopulation, and that is exactly what we saw (Figure 3.4, bottom left). Although the main effect of bin in the RMANOVA was just shy of statistical significance, ($F(2,52)=3.04, p=0.057$), a t-test of the within-cell change from baseline to late adaptation was marginally significant (-4.5 ± 2.21 Hz, $t(26) = -2.06$, $p=0.0499$). The observed changes in SS modulation during Tag 1 saccades in other (non-adapted) directions, however, were not significant according to either the RMANOVA ($F(2,52)=0.86$, $p=0.43$) or the t-test ($t(26)=-1.30$, $p=0.20$).

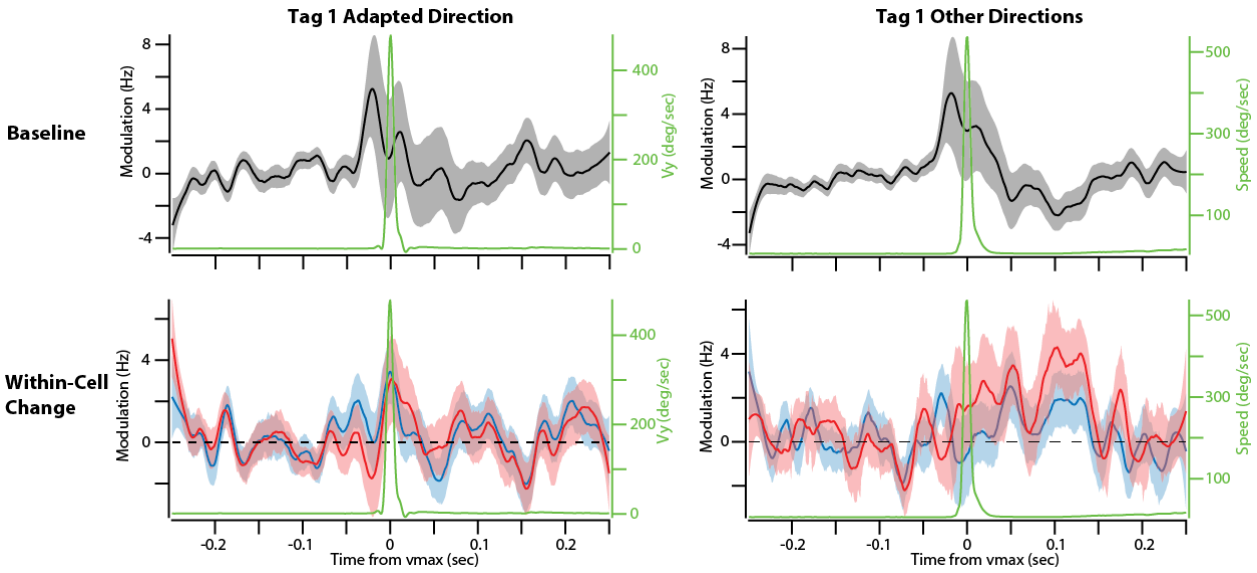


Figure 3.5 SS Modulation of the CS-off subpopulation. Top row is SS modulation during baseline period. Bottom row is the within cell change from baseline. Blue curve is early adaptation, and the red line is late adaptation. Left y-axes show modulation in Hz. Right y-axes show Vy (green curve) in the left column and speed in the right column. Data are aligned to peak speed (x-axes). Left column shows responses during upward Tag 1 (successful primary) saccades. There is an apparent but insignificant increase in the saccade related burst in late adaptation. Right column shows responses during Tag 1 saccades in all other directions with no apparent changes during adaptation.

Analyzing the saccade-related SS modulation in the CS-off cells subpopulation revealed a very similar SS burst during baseline for both Tag 1 saccades both in the upward direction and the other directions. However, the within-cell changes in the modulation are very different, as expected. Whereas an increase in CS firing rate causes LTD of SS for subsequent similar saccades, a decrease in CS firing rate results in LTP of the SS during subsequent saccades. However, this LTP due to lack of CS is smaller than the LTD due to abundance of CS, so we expected any increases in SS modulation in the CS-off subpopulation to be smaller/weaker than the changes we observed in the CS-on subpopulation. That is indeed what our results showed (Fig. 3.5, bottom row). There was no main effect of bin in the RMANOA for the CS-off cells during upward Tag 1 saccades ($F(2,80)=2.10$) $p=0.13$), and while there was a slight increase in SS modulation during the saccade, it did not reach statistical significance (2.60 ± 1.89 Hz, $t(40)=1.37$, $p=0.18$). Similarly, there was no main effect of bin ($F(2,80)=1.25$, $p=0.29$) or change in SS modulation during the non-adapted Tag 1 saccades (Figure 3.5, bottom right; $t(40)=1.09$, $p=0.28$).

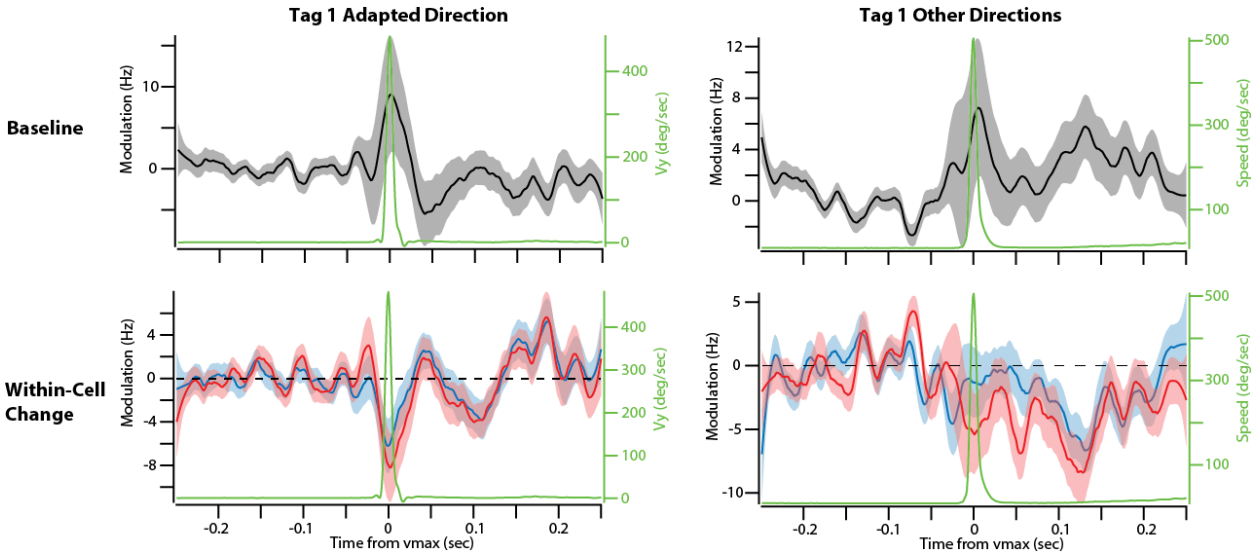


Figure 3.6 SS Modulation of the recombined population. Recombined population was formed by subtracting the mean activity of the CS-off subpopulation from the mean activity of the CS-on subpopulation. Top row is SS modulation during baseline period. Bottom row is the within cell change from baseline. Blue curve is early adaptation, and the red line is late adaptation. Left y-axes show modulation in Hz. Right y-axes show Vy (green curve) in the left column and speed in the right column. Data are aligned to peak speed (x-axes). Left column shows responses during upward Tag 1 (successful primary) saccades. There is clear LTD in late adaptation. Right column shows responses during Tag 1 saccades in all other directions. It also shows an apparent but insignificant reduction in SS modulation in late adaptation.

Next, we recombined the CS-on and CS-off subpopulations into the full population response (see Methods) and analyzed the saccade-related SS modulation during upward Tag 1 and downward Tag 6 saccades (Figure 3.6). As expected, we saw a saccade-related SS burst during the baseline period (Figure 3.6, top row). Also, as expected, the within-cell change during upward Tag 1 saccades for the population was robust (Figure 3.6, bottom left; -7.14 ± 2.86 Hz, 95% confidence interval (CI)=[-12.84 -1.63], p=0.02). Similar to the two subpopulations, the full population response did not show a significant change in SS modulation for non-adapted Tag 1 saccades (Figure 3.6, bottom right; -4.92 ± 2.82 Hz, 95% CI=[-10.41 0.79], p=0.08).

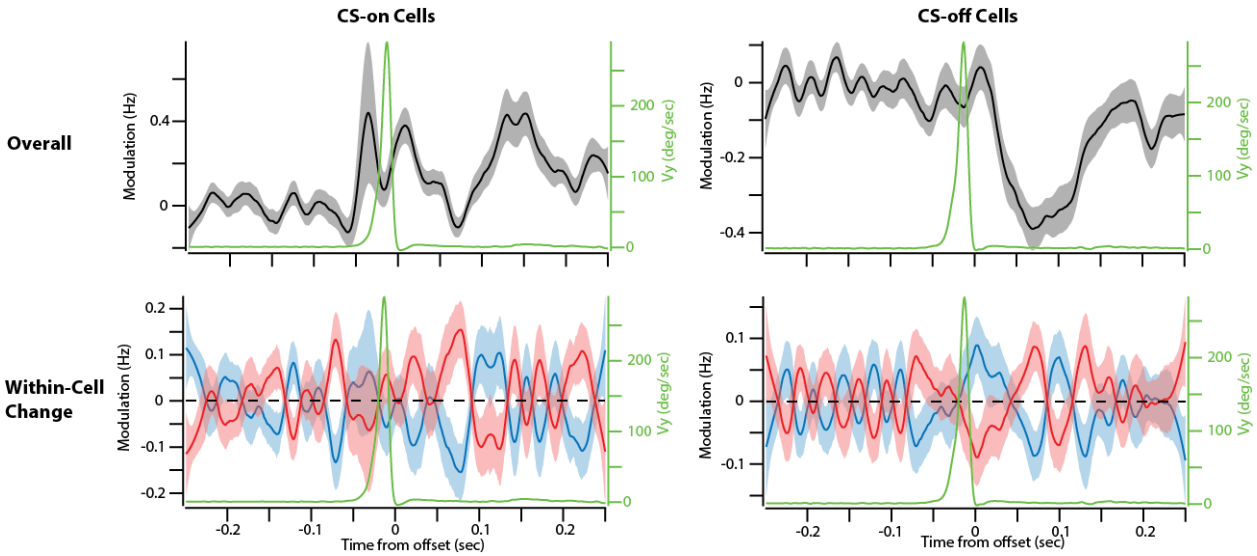


Figure 3.7. CS Response to Error. Left column shows CS-on subpopulation. Right column shows CS-on subpopulation. Left y-axes show modulation in Hz. Right y-axes show Vy (green curve). Data are aligned to the offset of upward Tag 1 (successful primary) saccades (x-axes). Top row is the mean CS modulation during the adaptation period. Bottom row is the within cell change from that mean comparing early adaptation (blue) to late adaptation (red). CS-on subpopulation shows a burst prior to saccade onset (perhaps in response to the target appearance), although this is absent in the CS-off subpopulation. As expected, the CS-on subpopulation shows a burst approximately 75ms after saccade offset when the brain should be registering the visual error (top left), whereas the CS-off subpopulation shows a pause (top right). There are no significant within cell changes for either subpopulation, and the variations appear to be sinusoidal noise.

Finally, we also examined changes in CS modulation (Figure 3.7). Rather than focusing on a time window during the saccade as we did for the SS modulation, we instead focused on the CS modulation during the 200ms after the offset of upward Tag 1 saccades since that is when the animal experiences the foveal error to which they adapted. There is a clear increase in CS firing rate in response to the error in the CS-on subpopulation (Figure 3.7, top left) and a clear reduction in the CS firing rate in the CS-off subpopulation (Figure 3.7, top right). Our dataset did not show a significant main effect of bin on CS modulation for the CS-on subpopulation ($F(2,76)=2.26$, $p=0.11$) but did for the CS-off subpopulation ($F(2,146)=11.73$, $p<0.001$). However, there were no significant within-cell changes in CS modulation for either subpopulation or the recombined population (CS-on Cells: 0.03 ± 0.05 Hz, $t(39)=0.76$, $p=0.45$; CS-off cells: 0.01 ± 0.04 Hz, $t(73)=0.24$, $p=0.81$; Population: 0.03 ± 0.06 Hz, 95% CI=[-0.09 0.14], $p=0.65$). We found this somewhat surprising given the significant adaptation to the intra-saccadic target jump and

the significant change in SS modulation, but it could be that the level of adaptation was too small (< 0.2^o from a 2.5^o target jump) to appreciably effect the CS response to the error.

Conclusions

We set out to test whether distinct subpopulations of P-cells in the OMV might support separate learning processes expressed early versus late in saccades. First, we demonstrated that our marmoset model was appropriate by measuring significant adaptation to the cross-axis perturbation in both animals and observed that a greater portion of this adaptation was expressed during the deceleration phase of the saccade than during the acceleration phase. Then, we showed that the changes in SS modulation of P-cells in the OMV were more robust in the CS-on subpopulation than the CS-off subpopulation and that the changes in each subpopulation were consistent with the observed CS response to the visual error within that subpopulation. Specifically, the CS-on subpopulation experienced an increase in CS firing rate in response to the visual error and showed a significant decrease in the saccade-related SS burst during adaptation. The CS-off subpopulation, on the other hand, experienced a decrease in CS firing rate in response to the visual error and showed an apparent but less than statistically significant increase in the saccade-related SS burst during adaptation. This provides initial evidence in support of our hypothesis, although further studies are needed.

Chapter 4: Conclusions and Future Directions

The ability to make accurate movements underpins many, if not all, of the tasks we perform in our everyday lives, and a loss of this ability causes a sharp drop in quality of life. Moreover, the cerebellum is believed to be essential to this ability, but the exact neural mechanisms behind its role remain poorly understood. This dissertation sought to contribute to the body of research on the cerebellum's role in motor control by advancing our knowledge of saccadic adaptation.

In Chapter 2, we described the results of 3 cross-axis saccade adaptation experiments in human subjects. In the first experiment, we found that the adaptation expressed during the deceleration phase of a saccade grows faster than the adaptation expressed during acceleration but suffers greater decay over time during breaks, despite the decay over trials during error clamp being identical across the two phases of the saccade. In the second experiment, we observed qualitatively similar patterns of adaptation and retention to the results of Experiment 1 but found that spontaneous recovery did not differ between acceleration and deceleration phases. Therefore, we concluded that both phases of the saccade must be supported by both a fast and a slow adaptation process. Finally, in Experiment 3, we showed that the adaptive response to a single error is confined to the deceleration phase of the movement. Overall, these experimental results suggest that there is a shared adaptation process expressed during both acceleration and deceleration as well as independent adaptation processes for each.

While these results are interesting and provide some evidence for distinct controllers active in adaptation expressed during different parts of the same saccade, there are still several questions that remain. First, if we manipulated the reaction time of saccades would that change the proportion of total adaptation expressed during acceleration versus deceleration? We thought that adaptation during acceleration could be related to re-aiming, which requires time to compute, greater reaction times

might increase the amount of adaptation expressed during acceleration. Second, why was there a slight exaggeration of the error during the acceleration phase of the adapted saccade in the single trial learning experiment? Is that exaggeration real or an artifact of our data? Further work is needed to begin answering these questions.

In Chapter 3, we detailed the results of our work in non-human primates, specifically the common marmoset. Like human subjects, these animals adapted to the cross-axis perturbation and expressed greater levels of adaptation during deceleration than acceleration. Moreover, analysis of the SS modulation in the OMV during adapted saccades suggested a relationship between changes in this modulation and the amount of adaptation the animals achieved, specifically a strong decrease in SS modulation in the CS-on subpopulation corresponded to strong behavioral adaptation, whereas a weaker increase in SS modulation in the CS-off subpopulation corresponded to weak adaptation. This is particularly striking given that we did not see any significant modulation or changes in the CS activity, in either subpopulation nor in the recombined population.

These results suggest many avenues for fruitful work in the future. First, one area we were unable to examine here is the role of synchrony in saccade adaptation. Recent work from the Shadmehr lab suggests that synchronous simple spikes are a powerful signal to the deep cerebellar nuclei, where the output neurons to the rest of the brain reside, and could therefore provide another mechanism for motor adaptation [36]. Likewise, the role of CS as a teaching signal remains unclear and merits further study. The fact that we saw stronger adaptation in the CS-on subpopulation than the CS-off subpopulation provides further support for CS firing as important for learning, but the lack of CS modulation in response to the visual error undermines that conclusion.

In summary, motor control and the role of the cerebellum remain a fascinating and promising area of research. This dissertation provided evidence that distinct subpopulations of P-cells may differentially contribute to motor adaptation depending on the relationship between their preferred

error direction and the error actually experienced and also raised more questions for future work. Hopefully, it can become yet another step in the quest to grow our knowledge of this fascinating and important topic.

References

1. Foulsham, T. Eye movements and their functions in everyday tasks. in *Eye (Basingstoke)* vol. 29 (2015).
2. Tian, J., Ying, H. S. & Zee, D. S. Revisiting corrective saccades: Role of visual feedback. *Vision Res* **89**, (2013).
3. Chen-Harris, H., Joiner, W. M., Ethier, V., Zee, D. S. & Shadmehr, R. Adaptive Control of Saccades via Internal Feedback. *Journal of Neuroscience* **28**, 2804–2813 (2008).
4. Robinson, D. A. Is the oculomotor system a cartoon of motor control? *Prog Brain Res* **64**, 411–417 (1986).
5. Wolpert, D. M. & Miall, R. C. Forward Models for Physiological Motor Control. *Neural Netw* **9**, 1265–1279 (1996).
6. Bhanpuri, N. H., Okamura, A. M. & Bastian, A. J. Predictive Modeling by the Cerebellum Improves Proprioception. *Journal of Neuroscience* **33**, 14301–14306 (2013).
7. Smith, M. A., Ghazizadeh, A. & Shadmehr, R. Interacting adaptive processes with different timescales underlie short-term motor learning. *PLoS Biol* **4**, 1035–1043 (2006).
8. Yang, Y. & Lisberger, S. G. Learning on Multiple Timescales in Smooth Pursuit Eye Movements. *J Neurophysiol* **104**, 2850–2862 (2010).
9. Joiner, W. M. & Smith, M. A. Long-term retention explained by a model of short-term learning in the adaptive control of reaching. *J Neurophysiol* **100**, 2948–55 (2008).
10. Ethier, V., Zee, D. S. & Shadmehr, R. Spontaneous recovery of motor memory during saccade adaptation. *J Neurophysiol* **99**, 2577–83 (2008).
11. Sarwary, A. M. E., Wischnewski, M., Schutter, D. J. L. G., Selen, L. P. J. & Medendorp, W. P. Corticospinal correlates of fast and slow adaptive processes in motor learning. *J Neurophysiol* **120**, (2018).
12. Inoue, M. *et al.* Three timescales in prism adaptation. *J Neurophysiol* **113**, (2015).
13. Stollhoff, N., Menzel, R. & Eisenhardt, D. Spontaneous recovery from extinction depends on the reconsolidation of the acquisition memory in an appetitive learning paradigm in the honeybee (Apis mellifera). *Journal of Neuroscience* **25**, (2005).
14. Schiller, D. *et al.* Preventing the return of fear in humans using reconsolidation update mechanisms. *Nature* **463**, (2010).
15. Mesik, J., Bao, M. & Engel, S. A. Spontaneous recovery of motion and face aftereffects. *Vision Res* **89**, (2013).
16. Mei, G., Yuan, Q., Liu, G., Pan, Y. & Bao, M. Spontaneous recovery and time course of biological motion adaptation. *Vision Res* **149**, (2018).
17. Noto, C. T. & Robinson, F. R. Visual error is the stimulus for saccade gain adaptation. *Brain Res Cogn Brain Res* **12**, 301–5 (2001).

18. Inaba, N., Iwamoto, Y. & Yoshida, K. Changes in cerebellar fastigial burst activity related to saccadic gain adaptation in the monkey. *Neurosci Res* (2003) doi:10.1016/S0168-0102(03)00098-1.

19. Belmeguenai, A. *et al.* Development/Plasticity/Repair Intrinsic Plasticity Complements Long-Term Potentiation in Parallel Fiber Input Gain Control in Cerebellar Purkinje Cells. (2010) doi:10.1523/JNEUROSCI.3226-10.2010.

20. Boyden, E. S., Katoh, A. & Raymond, J. L. CEREBELLUM-DEPENDENT LEARNING: The Role of Multiple Plasticity Mechanisms. *Annu. Rev. Neurosci* **27**, 581–609 (2004).

21. Tseng, Y. -w., Diedrichsen, J., Krakauer, J. W., Shadmehr, R. & Bastian, A. J. Sensory Prediction Errors Drive Cerebellum-Dependent Adaptation of Reaching. *J Neurophysiol* **98**, 54–62 (2007).

22. Sokolov, A. A., Miall, R. C. & Ivry, R. B. The Cerebellum: Adaptive Prediction for Movement and Cognition. *Trends in Cognitive Sciences* vol. 21 Preprint at https://doi.org/10.1016/j.tics.2017.02.005 (2017).

23. Carey, M. R. Synaptic mechanisms of sensorimotor learning in the cerebellum. *Current Opinion in Neurobiology* Preprint at https://doi.org/10.1016/j.conb.2011.06.011 (2011).

24. Darmohray, D. M., Jacobs, J. R., Marques, H. G. & Carey, M. R. Spatial and Temporal Locomotor Learning in Mouse Cerebellum. *Neuron* (2019) doi:10.1016/j.neuron.2019.01.038.

25. Lee, K. H. *et al.* Circuit mechanisms underlying motor memory formation in the cerebellum. *Neuron* **86**, 529–540 (2015).

26. Lang, E. J. *et al.* The Roles of the Olivocerebellar Pathway in Motor Learning and Motor Control. A Consensus Paper. *Cerebellum* **16**, 230–252 (2017).

27. Herzfeld, D. J. *et al.* Contributions of the cerebellum and the motor cortex to acquisition and retention of motor memories. *Neuroimage* **98**, (2014).

28. Soetedjo, R., Kojima, Y. & Fuchs, A. F. Complex spike activity in the oculomotor vermis of the cerebellum: A vectorial error signal for saccade motor learning? *J Neurophysiol* **100**, (2008).

29. Albergaria, C., Silva, N. T., Pritchett, D. L. & Carey, M. R. Locomotor activity modulates associative learning in mouse cerebellum. *Nat Neurosci* **21**, (2018).

30. Wagner, M. J. *et al.* Shared Cortex-Cerebellum Dynamics in the Execution and Learning of a Motor Task. *Cell* **177**, (2019).

31. Diedrichsen, J., King, M., Hernandez-Castillo, C., Sereno, M. & Ivry, R. B. Universal Transform or Multiple Functionality? Understanding the Contribution of the Human Cerebellum across Task Domains. *Neuron* vol. 102 Preprint at https://doi.org/10.1016/j.neuron.2019.04.021 (2019).

32. Rowan, M. J. M. *et al.* Graded Control of Climbing-Fiber-Mediated Plasticity and Learning by Inhibition in the Cerebellum. *Neuron* **99**, 999-1015.e6 (2018).

33. Herzfeld, D. J., Kojima, Y., Soetedjo, R. & Shadmehr, R. Encoding of action by the Purkinje cells of the cerebellum. *Nature* **526**, 439–42 (2015).

34. Herzfeld, D. J., Kojima, Y., Soetedjo, R. & Shadmehr, R. Encoding of error and learning to correct that error by the Purkinje cells of the cerebellum. *Nat Neurosci* (2018) doi:10.1038/s41593-018-0136-y.

35. Markanday, A., Inoue, J., Dicke, P. W. & Thier, P. Cerebellar complex spikes multiplex complementary behavioral information. *PLoS Biol* **19**, (2021).

36. Sedaghat-Nejad, E., Pi, J. S., Hage, P., Fakharian, M. A. & Shadmehr, R. Synchronous spiking of cerebellar Purkinje cells during control of movements. *Proc Natl Acad Sci U S A* **119**, (2022).

37. Golla, H. *et al.* Reduced saccadic resilience and impaired saccadic adaptation due to cerebellar disease. *European Journal of Neuroscience* **27**, (2008).

38. Xu-Wilson, M., Chen-Harris, H., Zee, D. S. & Shadmehr, R. Cerebellar contributions to adaptive control of saccades in humans. *J Neurosci* **29**, 12930–9 (2009).

39. Kojima, Y., Iwamoto, Y. & Yoshida, K. Memory of Learning Facilitates Saccadic Adaptation in the Monkey. *Journal of Neuroscience* **24**, 7531–9 (2004).

40. Ethier, V., Zee, D. & Shadmehr, R. Spontaneous recovery of motor memory during saccade adaptation. doi:10.1152/jn.00015.2008.

41. Criscimagna-Hemminger, S. E. & Shadmehr, R. Consolidation patterns of human motor memory. *Journal of Neuroscience* **28**, (2008).

42. Bao, M. & Engel, S. A. Distinct mechanism for long-term contrast adaptation. *Proc Natl Acad Sci U S A* **109**, (2012).

43. Kording, K. P., Tenenbaum, J. B. & Shadmehr, R. The dynamics of memory as a consequence of optimal adaptation to a changing body. *Nat Neurosci* **10**, (2007).

44. Herzfeld, D. J., Vaswani, P. A., Marko, M. K. & Shadmehr, R. A memory of errors in sensorimotor learning. *Science (1979)* **345**, 1349–1353 (2014).

45. Casellato, C. *et al.* Distributed cerebellar plasticity implements generalized multiple-scale memory components in real-robot sensorimotor tasks. *Front Comput Neurosci* **9**, (2015).

46. Hall, N. J., Yang, Y. & Lisberger, S. G. Multiple components in direction learning in smooth pursuit eye movements of monkeys. *J Neurophysiol* **120**, (2018).

47. Mandelblat-Cerf, Y. *et al.* The neuronal basis of long-term sensorimotor learning. *Journal of Neuroscience* **31**, (2011).

48. Shadmehr, R. Population coding in the cerebellum: A machine learning perspective. *Journal of Neurophysiology* vol. 124 Preprint at https://doi.org/10.1152/jn.00449.2020 (2020).

49. Yamazakia, T., Nagao, S., Lennon, W. & Tanaka, S. Modeling memory consolidation during posttraining periods in cerebellovestibular learning. *Proc Natl Acad Sci U S A* **112**, (2015).

50. Yang, Y. & Lisberger, S. G. Role of plasticity at different sites across the time course of cerebellar motor learning. *Journal of Neuroscience* **34**, (2014).

51. Cassady, K. *et al.* Neural predictors of sensorimotor adaptation rate and savings. *Hum Brain Mapp* **39**, (2018).

52. Della-Maggiore, V., Villalta, J. I., Kovacevic, N. & McIntosh, A. R. Functional evidence for memory stabilization in sensorimotor adaptation: A 24-h resting-state fmri study. *Cerebral Cortex* **27**, (2017).

53. Galea, J. M., Vazquez, A., Pasricha, N., Orban De Xivry, J. J. & Celnik, P. Dissociating the roles of the cerebellum and motor cortex during adaptive learning: The motor cortex retains what the cerebellum learns. *Cerebral Cortex* **21**, (2011).

54. Hadipour-Niktarash, A., Lee, C. K., Desmond, J. E. & Shadmehr, R. Impairment of retention but not acquisition of a visuomotor skill through time-dependent disruption of primary motor cortex. *Journal of Neuroscience* **27**, (2007).

55. Hamel, R., Trempe, M. & Bernier, P. M. Disruption of M1 activity during performance plateau impairs consolidation of motor memories. *Journal of Neuroscience* **37**, (2017).

56. Kim, S., Ogawa, K., Lv, J., Schweighofer, N. & Imamizu, H. Neural Substrates Related to Motor Memory with Multiple Timescales in Sensorimotor Adaptation. *PLoS Biol* **13**, (2015).

57. Landi, S. M., Baguear, F. & Della-Maggiore, V. One week of motor adaptation induces structural changes in primary motor cortex that predict long-term memory one year later. *Journal of Neuroscience* **31**, (2011).

58. Li, J. X., Medina, J. F., Frank, L. M. & Lisberger, S. G. Acquisition of neural learning in cerebellum and cerebral cortex for smooth pursuit eye movements. *Journal of Neuroscience* **31**, (2011).

59. Medina, J. F., Garcia, K. S. & Mauk, M. D. A mechanism for savings in the cerebellum. *Journal of Neuroscience* **21**, (2001).

60. Ruitenberg, M. F. L. *et al.* Neural correlates of multi-day learning and savings in sensorimotor adaptation. *Sci Rep* **8**, (2018).

61. Trewartha, K. M., Garcia, A., Wolpert, D. M. & Flanagan, J. R. Fast but fleeting: Adaptive motor learning processes associated with aging and cognitive decline. *Journal of Neuroscience* **34**, (2014).

62. Villalta, J. I., Landi, S. M., Fló, A. & Della-Maggiore, V. Extinction interferes with the retrieval of visuomotor memories through a mechanism involving the sensorimotor cortex. *Cerebral Cortex* **25**, (2015).

63. Werner, S., Schorn, C. F., Bock, O., Theysohn, N. & Timmann, D. Neural correlates of adaptation to gradual and to sudden visuomotor distortions in humans. *Exp Brain Res* **232**, (2014).

64. Holland, P., Codol, O. & Galea, J. M. Contribution of explicit processes to reinforcement-based motor learning. *J Neurophysiol* **119**, (2018).

65. McDougle, S. D., Bond, K. M. & Taylor, J. A. Explicit and implicit processes constitute the fast and slow processes of sensorimotor learning. *Journal of Neuroscience* **35**, (2015).

66. Quaia, C., Paré, M., Wurtz, R. H. & Optican, L. M. Extent of compensation for variations in monkey saccadic eye movements. *Exp Brain Res* **132**, (2000).

67. Sparks, D. L., Barton, E. J., Gandhi, N. J. & Nelson, J. Studies of the role of the paramedian pontine reticular formation in the control of head-restrained and head-unrestrained gaze shifts. in *Annals of the New York Academy of Sciences* vol. 956 (2002).

68. Xu-Wilson, M., Tian, J., Shadmehr, R. & Zee, D. S. TMS perturbs saccade trajectories and unmasks an internal feedback controller for saccades. *Journal of Neuroscience* **31**, (2011).

69. Albert, S. T. *et al.* Competition between parallel sensorimotor learning systems. *Elife* **11**, (2022).

70. Leow, L. A., Marinovic, W., de Rugy, A. & Carroll, T. J. Task errors drive memories that improve sensorimotor adaptation. *Journal of Neuroscience* **40**, (2020).

71. Miyamoto, Y. R., Wang, S. & Smith, M. A. Implicit adaptation compensates for erratic explicit strategy in human motor learning. *Nat Neurosci* **23**, (2020).

72. Taylor, J. A., Krakauer, J. W. & Ivry, R. B. Explicit and Implicit Contributions to Learning in a Sensorimotor Adaptation Task. (2014) doi:10.1523/JNEUROSCI.3619-13.2014.

73. Quessy, S., Quinet, J. & Freedman, E. G. The locus of motor activity in the superior colliculus of the rhesus monkey is unaltered during saccadic adaptation. *Journal of Neuroscience* **30**, (2010).

74. Frens, M. A. & van Opstal, A. J. Monkey superior colliculus activity during short-term saccadic adaptation. *Brain Res Bull* **43**, (1997).

75. Takeichi, N., Kaneko, C. R. S. & Fuchs, A. F. Activity changes in monkey superior colliculus during saccade adaptation. *J Neurophysiol* **97**, (2007).

76. Gaymard, B., Rivaud-Péchoux, S., Yelnik, J., Pidoux, B. & Ploner, C. J. Involvement of the cerebellar thalamus in human saccade adaptation. *European Journal of Neuroscience* **14**, (2001).

77. Haith, A. M., Huberdeau, D. M. & Krakauer, J. W. The Influence of Movement Preparation Time on the Expression of Visuomotor Learning and Savings. *The Journal of Neuroscience* **35**, (2015).

78. Barash, S. *et al.* Saccadic dysmetria and adaptation after lesions of the cerebellar cortex. *J Neurosci* **19**, 10931–9 (1999).

79. Optican, L. M. & Robinson, D. A. Cerebellar-dependent adaptive control of primate saccadic system. *J Neurophysiol* **44**, (1980).

80. Panouillères, M. *et al.* Effects of structural and functional cerebellar lesions on sensorimotor adaptation of saccades. *Exp Brain Res* **231**, (2013).

81. Panouillères, M. *et al.* A role for the parietal cortex in sensorimotor adaptation of saccades. *Cerebral Cortex* **24**, (2014).

82. Sedaghat-Nejad, E. *et al.* Behavioral training of marmosets and electrophysiological recording from the cerebellum. *J Neurophysiol* **122**, (2019).

83. Medina, J. F. & Lisberger, S. G. Links from complex spikes to local plasticity and motor learning in the cerebellum of awake-behaving monkeys. *NATURE NEUROSCIENCE VOLUME* **11**, (2008).

84. Albert, S. T. & Shadmehr, R. The Neural Feedback Response to Error As a Teaching Signal for the Motor Learning System. *Journal of Neuroscience* **36**, (2016).

85. Brashers-Krug, T., Shadmehr, R. & Bizzi, E. Consolidation in human motor memory. *Nature* **382**, (1996).

86. Donchin, O., Francis, J. T. & Shadmehr, R. Quantifying generalization from trial-by-trial behavior of adaptive systems that learn with basis functions: Theory and experiments in human motor control. *Journal of Neuroscience* **23**, (2003).

87. Shadmehr, R. & Thoroughman, K. A. Learning of action through adaptive combination of motor primitives. *Nature* **407**, 742–747 (2000).

88. Soetedjo, R., Kojima, Y. & Fuchs, A. F. How cerebellar motor learning keeps saccades accurate. *J Neurophysiol* **121**, (2019).

89. Kaku, Y., Yoshida, K. & Iwamoto, Y. Learning signals from the superior colliculus for adaptation of saccadic eye movements in the monkey. *Journal of Neuroscience* **29**, (2009).

90. Soetedjo, R., Fuchs, A. F. & Kojima, Y. Subthreshold activation of the superior colliculus drives saccade motor learning. *Journal of Neuroscience* **29**, (2009).

91. Albert, S. T. & Shadmehr, R. Estimating properties of the fast and slow adaptive processes during sensorimotor adaptation. *J Neurophysiol* **119**, (2018).

92. Kojima, Y., Soetedjo, R. & Fuchs, A. F. Effects of GABA agonist and antagonist injections into the oculomotor vermis on horizontal saccades. *Brain Res* **1366**, 93–100 (2010).

93. Straube, A., Deubel, H., Ditterich, J. & Eggert, T. Cerebellar lesions impair rapid saccade amplitude adaptation. *Neurology* **57**, 2105–8 (2001).

94. Albus, J. S. A theory of cerebellar function. *Math Biosci* **10**, 25–61 (1971).

95. Marr, D. A theory of cerebellar cortex. *J Physiol* **202**, 437–470 (1969).

96. Ito, M. Neural design of the cerebellar motor control system. *Brain Res* (1972) doi:10.1016/0006-8993(72)90110-2.

97. Catz, N., Dicke, P. W. & Thier, P. Cerebellar complex spike firing is suitable to induce as well as to stabilize motor learning. *Current Biology* **15**, (2005).

98. Soetedjo, R. & Fuchs, A. F. Complex spike activity of Purkinje cells in the oculomotor vermis during behavioral adaptation of monkey saccades. *Journal of Neuroscience* **26**, (2006).

99. Kojima, Y., Soetedjo, R. & Fuchs, A. F. Changes in simple spike activity of some purkinje cells in the oculomotor vermis during saccade adaptation are appropriate to participate in motor learning. *Journal of Neuroscience* **30**, (2010).

100. Orozco, S. P., Albert, S. T. & Shadmehr, R. Adaptive control of movement deceleration during saccades. *PLoS Comput Biol* **17**, e1009176 (2021).

101. Siegle, J. H. *et al.* Open Ephys: An open-source, plugin-based platform for multichannel electrophysiology. *J Neural Eng* **14**, (2017).

102. Sedaghat-Nejad, E. *et al.* P-sort: An open-source software for cerebellar neurophysiology. *J Neurophysiol* **126**, (2021).

103. Pachitariu, M., Steinmetz, N., Kadir, S., Carandini, M. & Harris, K. D. *Kilosort: realtime spike-sorting for extracellular electrophysiology with hundreds of channels*. *bioRxiv* (2016).

CURRICULUM VITAE
The Johns Hopkins University School of Medicine

(Signature) _____ February 14, 2023
(Typed Name) Simon Orozco (Date of this version)

DEMOGRAPHIC AND PERSONAL INFORMATION

Personal Data

Business Address: 720 Rutland Ave, Traylor 416 Baltimore, MD 21205
Tel: 410-614-3424
E-mail: sorozco2@jhmi.edu

Education and Training

Year	Degree/Certificate, Discipline, Institution/City, Notes
Undergraduate	
2009	Bachelor of Arts, Biochemical Sciences, Harvard College
Doctoral/graduate	
2014	Master of Science, Biokinesiology, University of Southern California
2023	Doctor of Philosophy, Biomedical Engineering, Johns Hopkins University

PUBLICATIONS:

Original Research [OR]

Orozco SP, Albert ST, Shadmehr R (2021) Adaptive control of movement deceleration during saccades. PLoS Comput Biol 17(7): e1009176.

Sing GC, **Orozco SP**, & Smith MA. Limb motion dictates how motor learning arises from arbitrary environmental dynamics. J Neurophysiol. 2013 May;109(10):2466-82.

FUNDING

EXTRAMURAL Funding

Research Extramural Funding
Previous
4/1/2019 – 3/31/2022 Evidence of Multiple Timescales of Motor Memory within Single Movement
F31NS108731
NINDS
$146,572
Role: Investigator, 100%

RECOGNITION

Awards, Honors

2014 University of Southern California Order of Aretè, highest university award for graduating graduate students – based on campus and/or community leadership and academic merit

OTHER PROFESSIONAL ACCOMPLISHMENTS (*Optional)*

Posters (optional) (date, title sponsor, location, notes)

Orozco SP, Shadmehr R. Evidence of slow and fast learning processes in saccade adaptation. Society for Neuroscience (2019)

Orozco SP, Herzfeld D, Shadmehr R. Evidence of slow and fast learning processes in saccade adaptation. Society for Neuroscience (2018)

Orozco SP, Herzfeld D, Shadmehr R. Evidence of slow and fast learning processes in early and late halves respectively of saccades during cross-axis saccade adaptation. Society for Neuroscience (2017)

Orozco SP, Herzfeld D, Shadmehr R. Signatures of the fast and slow learning processes in the motor commands that move the eyes during a saccade. Neural Control of Movement (2017)